Geol. Mag. **149** (*3*), *2012, pp. 423–442. © Cambridge University Press 2011*
doi:10.1017/S001675681100094X

Provenance signatures for the Miocene volcaniclastic succession of the Tufiti di Tusa Formation, southern Apennines, Italy

FRANCESCO PERRI*†, SALVATORE CRITELLI*, FRANCESCO CAVALCANTE‡, GIOVANNI MONGELLI§, ROCCO DOMINICI*, MAURIZIO SONNINO* & ROSANNA DE ROSA*

*Dipartimento di Scienze della Terra, Università della Calabria, Arcavacata di Rende, 87036 Rende (CS), Italy
‡CNR – Istituto di Metodologie per l'Analisi Ambientale, 85050 Tito Scalo (PZ), Italy
§Dipartimento di Chimica, Università della Basilicata, Campus di Macchia Romana, 85100 Potenza (PZ), Italy

(*Received* 5 October 2010; *accepted* 11 March 2011; *first published online* 27 October 2011)

Abstract – The Tufiti di Tusa Formation, a siliciclastic turbidite system of lower Miocene age in southern Italy, is mainly composed of volcaniclastic and quartzolithic sandstones interbedded with mudrocks. Sandstones are subdivided into four distinctive petrofacies, evolving from quartzolithic to volcaniclastic lithofeldspathic and feldspatholithic, reflecting detrital evolution from growing orogen (quartzolithic petrofacies) to active volcanism (volcaniclastic petrofacies). The mineralogical composition of the associated mudrocks is predominantly characterized by phyllosilicates, mainly illite/smectite mixed layers (I/S R1 associated with minor amounts of I/S R0 in the lower part of the succession, and I/S R3 in its upper part), together with illite, detrital micas and chlorite, and minor amounts of chlorite/smectite mixed layers and kaolinite, in addition to quartz, calcite and feldspars. The most abundant phyllosilicates are I/S mixed layers, 10-Å minerals (illite and micas) and chlorite, while kaolinite and chlorite–smectite mixed layers are present as a few per cent or in trace amounts. X-ray diffraction patterns show the occurrence of the ordered I/S R1 mixed layers in most samples but, at the top of the succession, some samples are characterized by I/S R3 mixed layers, whilst in the lower part of the succession I/S R1 is associated with a lower amount of I/S R0. These features suggest that the Tufiti di Tusa Formation experienced a medium diagenetic grade, and the occurrence of I/S R3 could be explained by K-availability in samples in the upper part of the succession. The lithic fragments in sandstones are metasedimentary rocks of Palaeozoic age, and andesite to dacite volcanic rocks of early Miocene age. The associated mudrocks also contain trace element ratios (Cr/V, Y/Ni, La/Sc, Th/Sc, Th/Co, Th/Cr, Cr/Th and Eu/Eu*) consistent with a provenance containing intermediate to silicic sources with scarce or absent basic rocks. The chemical index of alteration (63.2 to 71.6) suggests a moderate degree of weathering in the source. Furthermore, the K/Cs ratios of sediments confirm likely moderate rather than intense weathering. The index of compositional variability (ICV) values (from 1.2 to 2.5) are high enough to suggest the mudrocks are first-cycle sediments with little recycling. The Al–Ti–Zr diagram and the Th/Sc v. Zr/Sc plot indicate poor sorting and rapid deposition of the sediments. Detrital and sedimentary evolution of the Tufiti di Tusa Formation provides constraints, in terms of relations between a growing orogenic system and active volcanism in the Central Mediterranean, to contribute to geodynamic and palaeogeographic reconstructions of the earliest collision in the southern Apennines region.

Keywords: provenance, composition, sandstone, mudrock, southern Apennines, Tufiti di Tusa Formation.

1. Introduction

Sandstone petrography and geochemical composition of shales have been used to constrain provenance of clastic supply and sedimentary evolution of sedimentary basins (e.g. Bhatia & Crook, 1986; Cullers, 2000; McLennan, Hemming & Hanson, 1993; Taylor & McLennan, 1985; Mongelli *et al*. 2006; Critelli *et al*. 2008; Perri *et al*. 2005, 2008, 2010; Caracciolo *et al*. 2009; Zaghloul *et al*. 2010). The mineralogy of shales and siltstones has also been used in determining the provenance and to check changes in the minerals derived from source rocks during weathering and diagenesis. Trace element ratios such as La/Sc, Th/Sc, Th/Co, Th/Cr, Cr/Th and Eu/Eu* have been used to distinguish sediments derived from different source rocks and to infer tectonic settings (McLennan, Hemming & Hanson, 1993). In particular, the relative amount of silicic to basic rock input from the source to shales and siltstones can be determined from ratios of trace elements that are concentrated in silicic source rocks (La and Th) relative to those that are concentrated in basic rocks (Co, Cr, Ni). Also, the size of the Eu anomaly (Eu/Eu*), LREE/HREE (light/heavy rare earth element) ratios and three-component trace element plots (e.g. La–Th–Sc) may also be used to determine the provenance of shales and siltstones as most basic rocks contain no negative Eu anomaly and often contain low LREE/HREE ratios, while more silicic rocks are more likely to contain a negative Eu

†Author for correspondence: perri@unibas.it

anomaly and often have high LREE/HREE ratios (e.g. Bhatia & Crook, 1986; Cullers, 2000 and many others). The Western Mediterranean Alpine region was marked during Miocene time by intense deformation and high pressure/low temperature (HP/LT) metamorphism (at pressures in the range of 0.8–2 GPa), followed by a retrograde phase associated with decompression, suggesting subduction and subsequent exhumation of continental crust. Thick synorogenic siliciclastic turbidite successions started to accumulate within the Apennine foreland basin system (e.g. the Tufiti di Tusa Formation) and in the Maghrebian and Betic Flysch troughs during late Oligocene to early Miocene times (Perrone *et al*. 2006 and references therein).

In this paper, we study the sandstone petrography and mudrock mineralogy and geochemistry of the lower Miocene volcaniclastic sediments of the Tufiti di Tusa Formation (Sicilide Complex; southern Apennines) and characterize their provenance signatures, climatic, geodynamic and palaeogeographic significance, and diagenetic evolution.

In southern Italy, the Sicilide Complex strata represent deposition in a remnant ocean basin related to the subduction of the Adria oceanic lithosphere beneath the Mesomediterranean microplate (e.g. Critelli, 1999; Guerrera, Martín-Algarra & Perrone, 1993; Critelli *et al*. 2008). This subduction was active during Miocene time, producing an accretionary prism, the Sicilide Complex, and calcalkaline volcanism above it, which is now preserved in Sardinia. The active volcanic source and the crystalline sources of the Calabria-Peloritani Terrane are recorded within the Sicilide foredeep, forming distinct early Miocene siliciclastic turbidite systems with sand compositions ranging from volcanolithic (Tufiti di Tusa Formation) to quartzolithic and quartzofeldspathic (Albanella, Corleto and Colle Cappella formations) (e.g. Critelli & Le Pera, 1998; Critelli, 1999). The volcanic source of sediment is mainly related to calcalkaline volcanic arcs (Guerrera & Veneri, 1989) or, more recently (latest Neogene–Quaternary), to intraorogenic alkaline volcanism. Lower Miocene (Burdigalian) foreland basin clastic sediments are widespread in the southern Apennines. Sediments of the upper Sicilide Complex represent the oldest deposits of the foredeep basin (Critelli, 1999).

2. Geology

The southern Apennines is an E-verging accretionary wedge developed in Neogene times above W-dipping subduction of the Apulian–Ionian lithosphere (Doglioni *et al*. 1996). The southern Apennines and northern Calabria are associated with the Tyrrhenian back-arc basin and bear today a frontal active accretionary wedge, below sea-level, whereas the main elevated ridge to the west is undergoing uplift and extension.

The tectonic style of the area is dominated by a large-scale duplex system, consisting of a complex architecture of tectonic units derived from the internal Apulia carbonate platform, overlain by a rootless thrust sheet derived from the western Adria palaeomargin and distally related oceanic basins (e.g. Patacca & Scandone, 2007 and references therein).

The subduction of the Tethyan oceanic lithosphere located to the west of the Adria margin was active in Oligocene and Miocene time, and was associated with calcalkaline volcanism coeval with intracontinental rifting occurring in Sardinia. Subduction-related volcanism (between 32 and 11 Ma) was widespread along the western side of Sardinia (e.g. Assorgia *et al*. 1986). This volcanism was subdivided into two main phases: calcalkaline eruptions of lavas from 32 to 26 Ma, and explosive eruptions, which alternated or were contemporaneous with effusive events, between 23 and 11 Ma (Boni, Del Vecchio & Lirer, 1990). The volcanic products of the first phase are andesite, basaltic andesite and basalt, whereas the second phase includes pyroclastic rocks from dacite to rhyolite composition.

According to different palaeogeographic restorations (Ogniben, 1969; Pescatore *et al*. 1999; Critelli, 1999; Patacca & Scandone, 2007 and many others), the southern Apenninic tectonic units derive from deformation of different palaeogeographic domains, represented, from west to east, by the Liguride–Sicilide basin (Flysch Domain), the Apennine carbonate platform, the Lagonegro basin and the Apulian carbonate platform (External Domain). In addition, the Internal Domain is represented by the metamorphic units of the Calabria–Peloritani Terrane, which does not crop out in the study area, but far towards the SW (Bonardi *et al*. 2001). The Liguride basin was formed on Tethyan oceanic crust, which was bounded, on its western and eastern sides, by continental crust belonging to the Internal (Calabria–Peloritani Terrane) and External Domains (Adria margin), respectively. The Adria margin includes the Apennine platform that was formed on the continental crust at the western margin, and towards the east the Lagonegro basin and the Apulian platform (e.g. Sgrosso, 1994 and references therein). The Lagonegro basin was located between the Apennine platform to the west and the Apulian platform to the east, the latter representing the proximal zone of the west Adria palaeomargin (e.g. Pescatore *et al*. 1999; Patacca & Scandone, 2007). The Sicilide Unit has been interpreted as representing deposition on the eastward flank of the Tethyan oceanic basin (e.g. Ogniben, 1969; Critelli, 1999; Lentini *et al*. 2002; Cavalcante *et al*. 2003; Patacca & Scandone, 2007).

The studied area is located in the Sicilide Unit cropping out at the front of the southern Apennines near Valsinni village (Fig. 1). In this sector, the Sicilide Unit overlies the Sannio Unit and is covered unconformably by Plio-Pleistocene siliciclastic sediments of the Bradano Trough (Patacca & Scandone, 2007 and references therein). Information on depositional characteristics and ages of the stratigraphic sequences representative of the thrust sheets and thrust-sheet-top deposits of the southern Apennines close to the studied area is given in a synoptic scheme (Fig. 2).

https://doi.org/10.1017/S001675681100094X Published online by Cambridge University Press

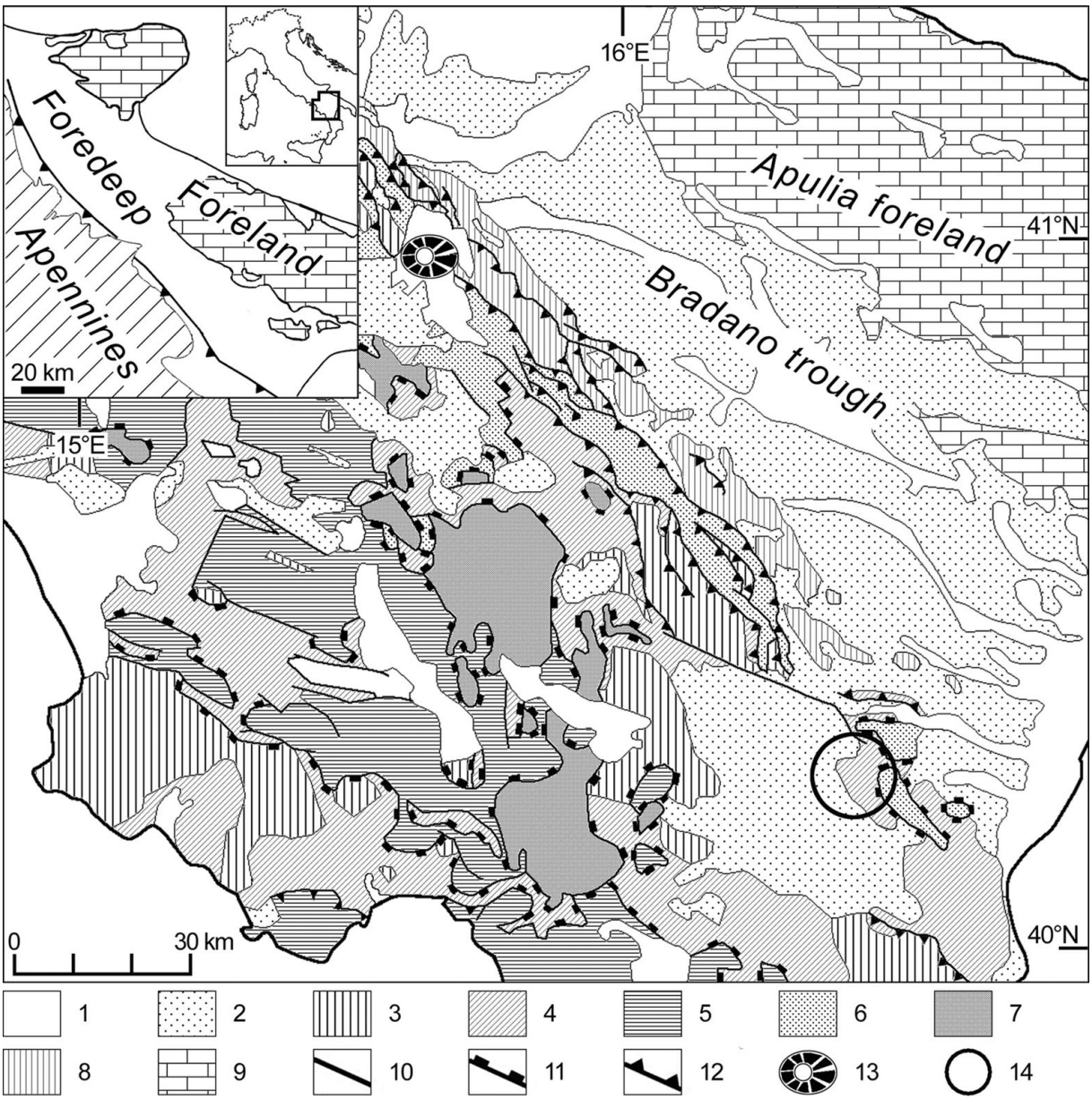

Figure 1. Geological sketch map of the southern Apennine and location of the studied area (modified from Patacca & Scandone, 2007). 1 – Continental and coastal deposits; volcanic rocks and volcaniclastic deposits (Holocene–middle Pleistocene). 2 – Middle Pleistocene–Pliocene thrust-top deposits. Terrigenous marine and paralic deposits filling the Bradano trough and unconformably overlying the Apennine Units. 3 – Miocene deposits (Gessosso–Solfifera Formation, San Bartolomeo Formation, Gorgoglione Formation, Albidona Formation). 4 – North Calabrian and Sicilide Units (lower Miocene–Cretaceous). 5 – Aburno-Cervati, Monti della Maddalena and minor units derived from the Campania–Lucania carbonate platform (lower Miocene–Upper Triassic). 6 – Sannio Unit (middle Miocene–Lower Cretaceous). 7 – Lagonegro Unit (Lower Cretaceous–Middle Triassic). 8 – Tufillo–Serra Palazzo and Daunia units (upper Miocene–Palaeogene). 9 – Cretaceous carbonates of the Murge foreland. 10 – Faults, including normal faults, lateral ramp and strike-slip faults. 11 – Low-angle thrust. 12 – High-angle thrust. 13 – Caldera rim (Vulture Volcano). 14 – Studied area.

The Sicilide Unit, established in the southern Apennines by Ogniben (1969), is widespread in the Basilicata region. The Sicilide stratigraphic succession, in the northern sector of the Basilicata region, consists of lower Cretaceous varicoloured clay and the Paleocene–lower Miocene Corleto-Perticara Formation, whereas in the studied area it consists of upper Cretaceous varicoloured clay, the Maastrichtian–lower Eocene Monte S. Arcangelo Formation, upper Eocene–lower Miocene varicoloured clay and lower Miocene Tufiti di Tusa Formation (e.g. Patacca & Scandone, 2007 and references therein). Siliciclastic strata of the Sicilide Complex include quartzolithic, volcanolithic and quartzofeldspathic sandstones (Critelli, 1999).

The studied succession consists of a nearly 100 m thick alternating sequence of volcaniclastic, calciclastic and quartzolithic turbidite strata. The sequence can be divided into two main parts based on both compositional and depositional characters: a lower fine-grained sandstone–mudstone part of calciclastic and quartzolithic composition, characterized by discontinuous and disorganized terrigenous supply; and an

https://doi.org/10.1017/S001675681100094X Published online by Cambridge University Press

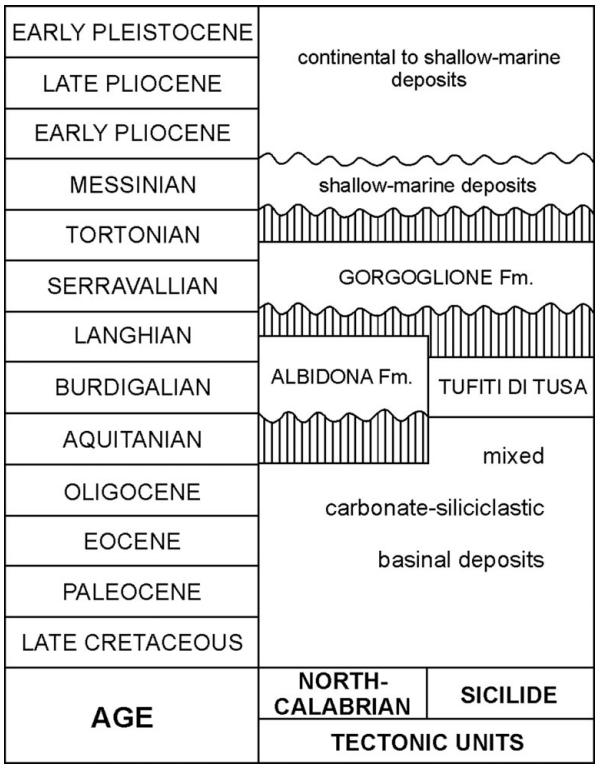

Figure 2. Synoptic scheme of depositional characteristics and ages of the stratigraphic sequences representative of the thrust sheets and thrust-sheet-top deposits of the southern Apennines close to the studied area (modified from Patacca & Scandone, 2007).

upper part, mostly of volcaniclastic composition, characterized by fine-grained yellow and grey sandstones with low-angle cross-bedding passing into parallel-laminated sandstones with some conglomerate beds alternating with grey centimetric mudrocks. The studied mudrock and sandstone samples were collected along the upper part of the stratigraphic succession (Fig. 3). The volcaniclastic turbidite strata form a thickening and coarsening upward sequence, and represent higher energy events of the stratigraphic succession (e.g. Critelli *et al*. 1990). Thick volcanolithic strata of the Tufiti di Tusa include syneruptive andesite and basaltic andesite sandstones, recording the climax of the calcalkaline volcanic arc activity (Critelli *et al*. 1990). Interbedded with carbonatoclastic sequences of the Adria forebulge (Capaccio–Roccadaspide and Cerchiara formations), similar andesitic volcanolithic sand testifies to wide dispersal of the neovolcanic detritus in the forebulge and back-bulge depozones (Critelli, 1999). Metamorphiclastic quartzolithic sandstones occur in the lower portions of the Tufiti di Tusa before deposition of volcaniclastic strata (Critelli *et al*. 1990). Thick carbonate (calcarenite-marl) turbidite strata are interbedded with quartzolithic and volcaniclastic strata of the Tufiti di Tusa Formation, testifying to provenance from the flexed forebulge domain (Critelli, 1999). Thus, the Tufiti di Tusa Formation caps the Sicilide Complex (Burdigalian–early Langhian) and represents the oldest sedimentary succession of the foredeep basin (e.g. Critelli, 1999).

3. Sampling and methods

To obtain a representative suite of samples from the Tufiti di Tusa Formation, a set of 18 mudrocks (FP123-FP140) and 16 sandstones (T1-T16) were collected along the Canale Coppozzolo stratigraphic succession near Valsinni village (Fig. 1). Samples were collected from the bottom to the top of the studied succession (Fig. 3).

Mudrock samples were cleaned for geochemical and mineralogical analyses. Weathered coats and veined surfaces were removed. The rocks were crushed and milled in an agate mortar to a very fine powder.

3.a. X-ray diffraction (XRD) analyses

The powdered samples were placed in an ultrasonic bath for a few minutes for disaggregation; the $< 2\ \mu m$ grain-size fraction was then separated by settling in distilled water. The mineralogy of the whole-rock and of the fine fractions ($< 2\ \mu m$) were determined by X-ray diffraction (XRD) using a Rigaku D/max 2200 diffractometer (Cu-Kα radiation; graphite secondary monochromator; sample spinner; step size, 0.02; speed, 3 sec steps). Oriented mounts were prepared, after Sr-saturation of the clay fraction, by evaporation of a clay-water suspension on the glass slides. XRD analyses were carried out on air-dried specimens, glycolated at 60 °C for 8 hours, and heated at 375 °C for 1 hour (Moore & Reynolds, 1997).

Quantitative mineralogical analysis of the bulk rock was carried out on random powders measuring peak areas for each mineral using the WINFIT computer program (Krumm, 1996). The strongest reflection of each mineral was considered, except for quartz for which the line at 4.26 Å was used instead of the peak at 3.34 Å because of its superimposition on that of the 10-Å minerals and of the I/S mixed layer series. The amount of phyllosilicates was estimated measuring the 4.5 Å peak area. The percentage of phyllosilicates in the bulk rock was split on the diffraction profile of the random powder, according to the following peak areas: 10–15 Å (I/S mixed layers), 10 Å (illite + micas) and 7 Å (kaolinite + chlorite) minerals (e.g. Cavalcante *et al*. 2007; Perri, 2008). The amount of these latter phases was estimated by considering the height of the peaks at 3.58 Å and 3.53 Å, respectively. The percentage of clay minerals in the $< 2\ \mu m$ fraction was estimated by measuring the peak areas on diffraction profiles of the glycolated and heated oriented mounts and considering the height of the peaks at 3.58 Å and 3.53 Å on diffraction profiles of the heated oriented specimens (Laviano, 1987).

The percentage of illite (%I) and stacking order (Reichweite; R) of the I/S mixed layers was determined on the spectrum of the glycolated specimens according to Moore & Reynolds (1997). The 2θ peak position was determined by decomposition of X-ray pattern using asymmetric and symmetric function at low and high angles, respectively. Experimental X-ray profiles were

https://doi.org/10.1017/S001675681100094X Published online by Cambridge University Press

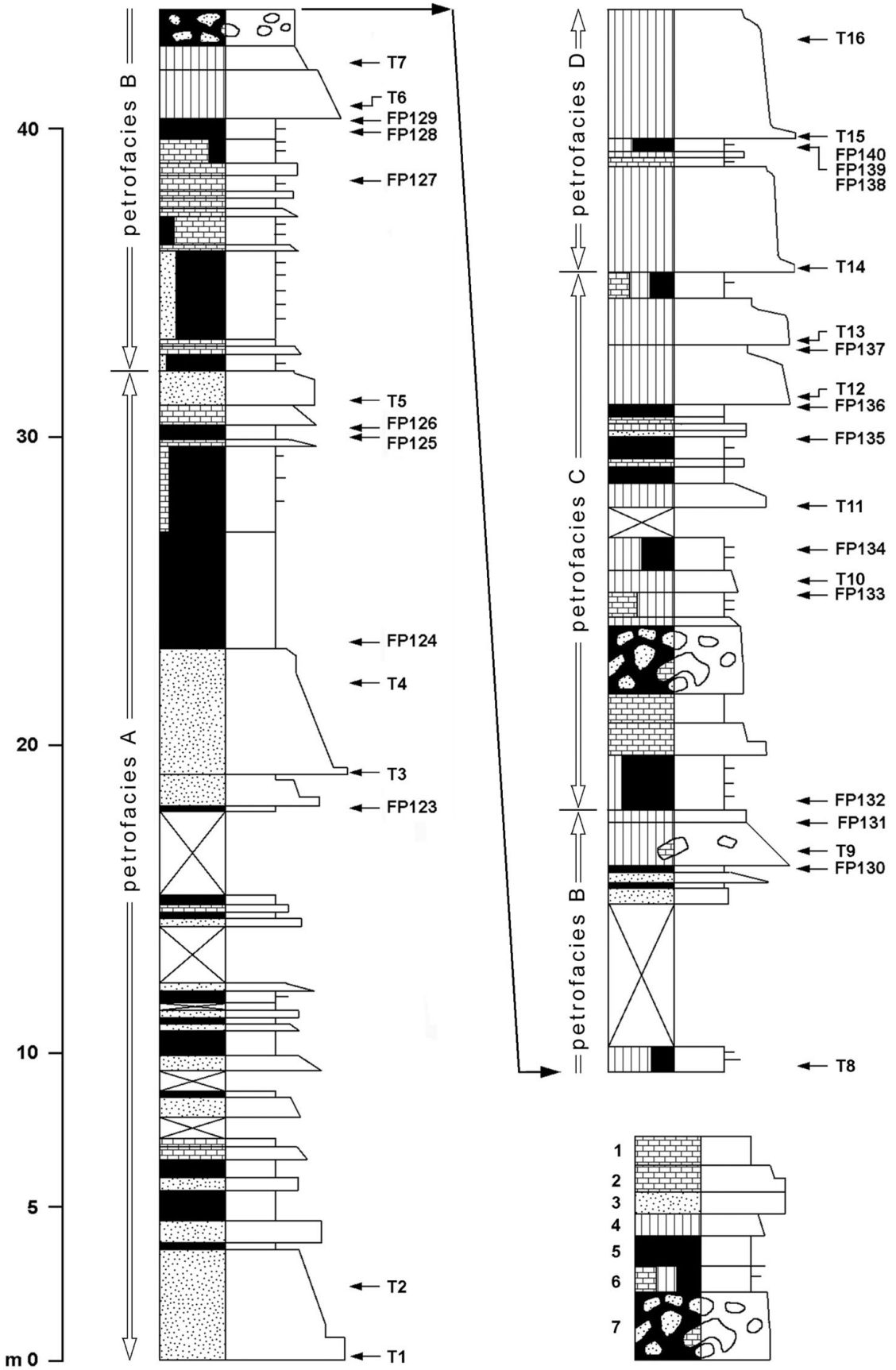

Figure 3. Sedimentological log of the volcaniclastic and carbonatoclastic deposits at the Canale Coppozzolo stratigraphic succession near Valsinni village, with the location of the studied mudrock (from FP123 to FP140) and sandstone (from T1 to T16) samples. 1 – calcilutites and marls; 2 – calciclastic sandstones; 3 – quartzolithic sandstones; 4 – volcaniclastic sandstones; 5 – mudrock; 6 – sandstone; 7 – slumping and debris flow bed. The sandstone petrofacies (A, B, C and D) are shown.

https://doi.org/10.1017/S001675681100094X Published online by Cambridge University Press

Table 1. Trace element concentration of the standard rocks that were run together with the studied mudrocks, at the Activation Laboratories (Ancaster, Canada)

Analyte Symbol	Cs	Hf	Sc	Th	U	Zn	La	Ce	Nd	Sm	Eu	Tb	Yb	Lu
Unit Symbol	ppm	ppm	ppm	ppm	ppm	ppm	ppm	ppm	ppm	ppm	ppm	ppm	ppm	ppm
Analysis Method	INAA	INAA	INAA	INAA	INAA	INAA	INAA	INAA	INAA	INAA	INAA	INAA	INAA	INAA
WMG-1 Meas	0.2	1.7	26.9	1.3	0.1	120	8.2	16	9	2.3	0.8	0.3	1.3	0.22
WMG-1 Cert	0.48	1.3	26	1.1	0.65	110	8.2	16	9	2.3	0.82	0.3	1.3	0.21
WMG-1 Meas	0.2	1.4	26.6	1.4	0.1	120	8.3	16	9	2.3	0.8	0.1	1.3	0.22
WMG-1 Cert	0.48	1.3	26	1.1	0.65	110	8.2	16	9	2.3	0.82	0.3	1.3	0.21

Table 2. Petrofacies of the studied sandstone samples

		Qm F Lt %			Qt F Lt %			Qm P K %			Qp Lv Lsm %				
Petrofacies		Qm	F	Lt	Qt	F	Lt	Qt	P	K	Qp	Lv	Lsm	P/F	Lv/L
Petr. A	av	46	18	36	46	18	36	72	26	2	–	41	59	0.9	0.41
	SD	18	3	16	18	38	16	9	9	1	–	30	30	0.01	0.30
Petr. B	av	14	15	71	14	15	71	36	63	1	–	83	17	1.0	0.83
	SD	8	7	5	8	7	5	21	22	3	–	7	7	0.01	0.68
Petr. C	av	17	26	57	17	36	57	31	69	–	–	84	16	1.0	0.82
	SD	5	6	6	5	6	6	9	9	–	–	11	11	0	0.11
Petr. D	av	10	52	38	10	52	38	16	84	–	–	92	8	1.0	0.92
	SD	3	2	2	3	2	2	2	2	–	–	2	2	0	0.02

Qm – monocrystalline quartz; F – feldspars; Lt – aphanitic lithic fragments; Qt – total quartz; Qp – polycrystalline quartz; Lv – volcanic and metavolcanic lithic fragments; Lsm – sedimentary and metasedimentary lithic fragments; P – plagioclase; K – K-feldspar; L – lithic fragments; av – average; SD – standard deviation.

compared with theoretical patterns calculated with the NEWMOD© computer program (Reynolds, 1985).

3.b. Geochemical analyses

Elemental analyses for major and some trace element (Nb, Zr, Y, Sr, Rb, Ba, Ni, Co, Cr, V) concentrations were obtained by X-ray fluorescence spectrometry (Philips PW 1480) at the Università della Calabria (Italy), on pressed powder discs of whole-rock samples and compared to international standard rock analyses of the United States Geological Survey. X-ray counts were converted into concentrations by a computer program based on the matrix correction method according to Franzini, Leoni & Saitta (1975) and Leoni & Saitta (1976). Loss on ignition (LOI) was determined after heating the samples for three hours at 900 °C. Instrumental Neutron Activation Analysis (INAA) at the Activation Laboratories (Ancaster, Canada) was used to determine the abundance of the REEs and Sc, Zn, Cs, Th, Hf and U. Trace element concentration of the standard rocks is shown in Table 1. The estimated precision and accuracy for trace element determinations are better than 5 %, except for those elements having a concentration of 10 ppm or less (10–15 %).

3.c. Petrography

Sixteen samples of unaltered medium-to-coarse sandstones were selected for thin-section analysis, covering the entire sedimentary succession. Thin-sections were prepared for these samples and were examined through a standard polarizing microscope. Thin-sections were etched and stained using hydrofluoric acid and sodium cobaltinitrite for plagioclase and potassium feldspar identification, respectively. The petrographic classes were recognized through quantitative petrographic point counting of the thin-sections, using the Gazzi–Dickinson method (Ingersoll *et al*. 1984), and according to the petrographic classes defined by Zuffa (1980) (Table 2). The composition of the 16 sandstone samples is based on 245–582 points per thin-section at a spacing of 0.5 mm.

3.d. Scanning electron microscopy (SEM)

Samples of selected mudrocks and sandstones were gold coated and analysed using a SEM-EDX (ESEM Philips Electronics QUANTA 200F with EDX GENESIS 4000).

4. Petrography

Sandstones include dominantly volcanic (Fig. 4a–e) detritus, even if plutonic, metamorphic and extrabasinal carbonate detritus is also present (Fig. 4f, g). Volcanic detritus is mainly represented by single phenocrysts and lithic fragments. The metamorphic detrital grains are mainly high-grade metamorphic fragments of quartz and feldspar with biotite, amphibole and epidote. Subordinate low-grade metamorphic fragments are phyllites and schists (Fig. 4h). Phaneritic plutonic fragments are exclusively quartz and feldspar. Extrabasinal carbonates include biomicritic, biosparitic and sparitic limestone fragments (Fig. 4f, g). Intrabasinal carbonate particles include coeval plankton tests and intraclasts. The volcaniclastic interstitial component is mainly characterized by a non-carbonatic pseudomatrix (*sensu* Dickinson, 1970) related to early diagenesis of volcanic detrital components.

Framework compositions of the studied sandstones can be subdivided into four distinctive petrofacies

https://doi.org/10.1017/S001675681100094X Published online by Cambridge University Press

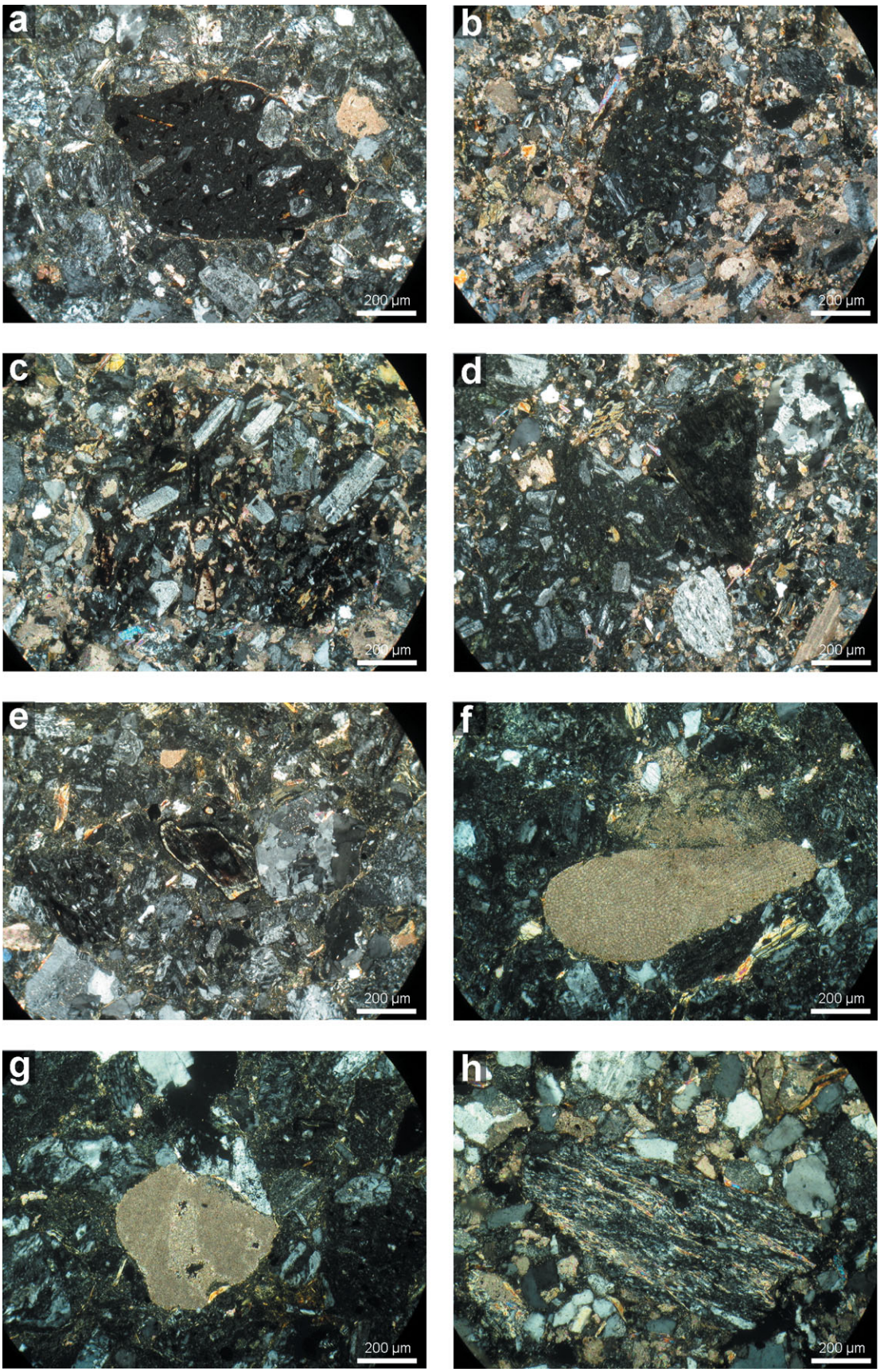

Figure 4. (Colour online) Photomicrographs of sand grains of the Tufiti di Tusa sandstones. (a, b) Volcanic lithic fragments; (c–e) microlitic texture (volcanic lithic grains with plagioclase phenocrystals); (f, g) carbonate extrabasinal grains; (h) phyllite fragments.

https://doi.org/10.1017/S001675681100094X Published online by Cambridge University Press

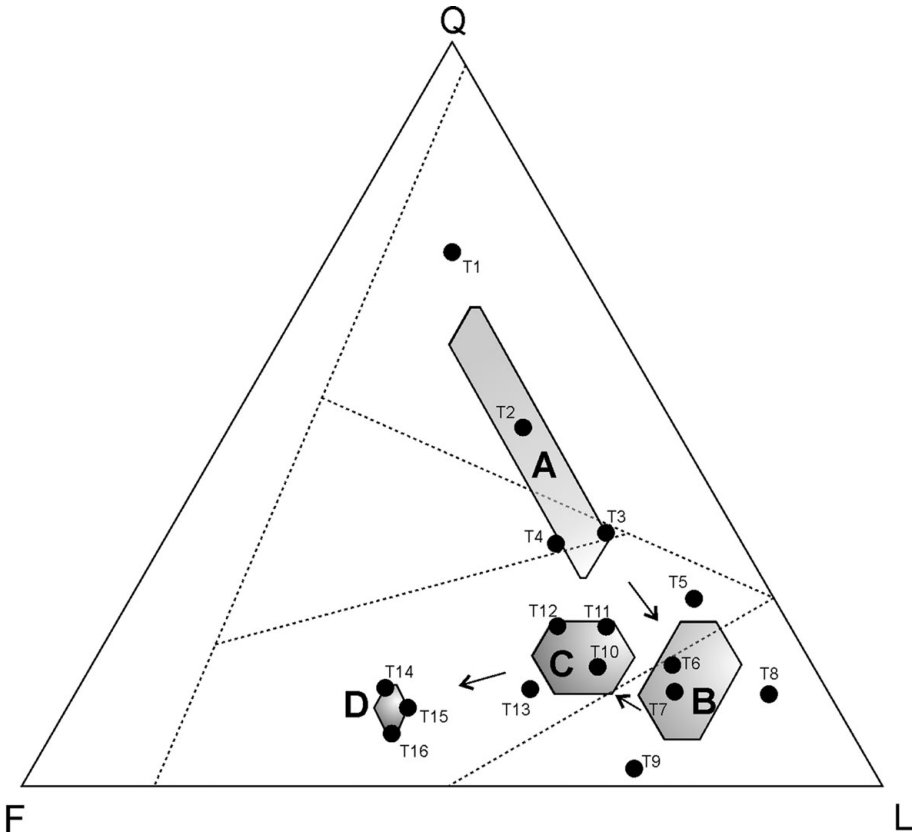

Figure 5. Triangular plot (after Zuffa, 1980; Ingersoll *et al*. 1984; Dickinson, 1985) of the sandstone samples from the Tufiti di Tusa Formation. From T1 to T16 – sandstone samples; A, B, C, D – petrofacies; Q – monocrystalline and polycrystalline quartz; F – feldspars; L – lithic fragments.

(*sensu* Dickinson, 1985), marking the compositional evolution of the Tufiti di Tusa Formation (Table 2; Fig. 5).

Petrofacies A (samples T1–T5) is quartzolithic in composition (Q_{46}–F_{18}–L_{36}), with abundant medium- and high-grade metamorphic fragments (Table 2) where volcanic detritus is minor. This petrofacies represents the basal portions of the formation.

Petrofacies B (samples T6–T9) is lithofeldspathic volcaniclastic in composition (Q_{14}–F_{15}–L_{71}) with P/F = 1 and a high Lv/L ratio (Table 2). Volcanic grains have dominantly microlitic and felsitic seriate textural attributes suggesting a provenance from andesitic volcanism. This petrofacies represents the middle portions of the formation.

Petrofacies C (samples T10–T13) is lithofeldspathic (Q_{17}–F_{26}–L_{57}) with P/F = 1 and a high Lv/L ratio (Table 2), containing dominantly volcanic detritus. This petrofacies includes abundant microlitic and felsitic seriate volcanic textures, such as vitric volcanic textures and single euhedral amphibole and plagioclase crystals. This petrofacies represents the middle–upper portions of the formation.

Petrofacies D (samples T14–T16) is feldspatholithic (Q_{10}–F_{52}–L_{38}) with P/F = 1 and a high Lv/L ratio (Table 2). This petrofacies includes abundant microlitic and felsitic seriate volcanic textures and single euhedral crystals of amphibole. Fine-grained strata of siltstone and mudrock interbedded with sandstone of this petrofacies consist exclusively of volcanic shards and pumice, and represent fine-grained ash turbidites. This petrofacies represents the upper portions of the formation.

The detrital modes of these arenites evolve from quartzolithic sandstones to lithofeldspathic and feldspatholithic sandstones.

The four petrofacies testify to an evolution from collisional orogen (petrofacies A) to volcanic arc (petrofacies B, C, D) (Fig. 5). The compositional evolution of the Tufiti di Tusa Formation is quite different to the general trend of circum-Pacific arc-trench systems related to volcanic-plutonic arc provenance (Dickinson, 1985).

5. Mudrock mineralogy

5.a. Bulk rock composition

The results of whole-rock XRD analyses are reported in Table 3. Non-phyllosilicate minerals are represented by quartz, calcite and feldspars. Gypsum was detected in a few samples. Quartz has concentrations ranging from 13 % to 41 %. Feldspars are present in low abundances, which increases towards the top. This trend is quite similar to the above-mentioned evolution of the sandstone petrofacies. The amount of calcite is variable and shows an average value of 12.4 %. The phyllosilicates are the main mineralogical components,

https://doi.org/10.1017/S001675681100094X Published online by Cambridge University Press

Table 3. Mineralogical composition of the bulk mudrock (wt %)

Samples	Σphy	Feld	Dol	Calc	Qtz	Gyp	I/S	Ill	C/S	Kao	Chl
FP123	56	1	0	30	13	0	38	11	3	0	5
FP124	49	2	0	23	26	0	17	18	0	0	17
FP125	63	0	0	19	17	0	43	11	2	2	6
FP126	66	0	0	18	16	0	39	12	4	6	8
FP127	50	1	0	29	19	0	38	5	1	0	4
FP128	66	1	0	11	22	1	50	8	2	3	4
FP129	65	2	0	8	26	0	27	16	6	0	18
FP130	66	0	0	12	22	0	52	7	1	0	7
FP131	53	2	0	14	31	0	26	12	1	0	15
FP132	61	2	0	5	32	0	35	12	0	2	12
FP133	66	2	0	6	24	2	42	18	0	0	7
FP134	55	2	0	8	35	0	14	25	0	0	17
FP135	52	4	0	7	38	0	31	9	1	2	9
FP136	57	3	0	9	31	0	38	12	0	0	8
FP137	47	7	0	6	41	0	19	14	2	2	9
FP138	57	3	0	2	38	0	35	17	0	0	6
FP139	52	3	0	13	33	0	40	6	2	1	3
FP140	55	3	0	4	39	0	27	15	2	2	10
minimum	47	0	0	2	13	0	14	5	0	0	3
maximum	66	7	0	30	41	2	52	25	6	6	18
average	57	2	0	12	28	0	34	13	2	1	9
SD	6	2	0	8	8	1	11	5	2	2	5

Qtz – quartz; Feld – feldspars (K-feldspars + plagioclase); Dol – dolomite; Calc – calcite; Σphy – sum of phyllosilicates; Gyp – gypsum; I/S – illite/smectite mixed layers; Ill – illite; C/S – chlorite/smectite mixed layers; Kao – kaolinite; Chl – chlorite; SD – standard deviation.

ranging from 47 % to 66 % of the bulk rock; the highest values are present in the middle–low stratigraphic interval. The I/S mixed layers are the most abundant phyllosilicates, ranging from 14 % to 52 %. The contents of 10-Å minerals (illite and micas) and chlorite range from a few per cent to 25 % and 18 %, respectively. The kaolinite and chlorite/smectite (C/S) mixed layers are present as a few per cent or in trace amounts, and are not detected in some samples.

5.b. Clay mineralogy

The < 2 μm grain-size fraction (Table 4) is mainly composed of I/S mixed layers (73–96 % in weight). Illite is present in variable amounts, from a few per cent up to 18 %. Chlorite contents are usually low. Kaolinite and C/S mixed layers are present in very low or trace percentages in many samples (Table 4).

As regarding the illite percentage in I/S mixed layers and the stacking order *R*, XRD patterns of the glycolated oriented slides show the occurrence of the ordered I/S R1 mixed layers in all samples, with illite percentage ranging from 65 % to 85 %, except for three samples collected from the top of the succession, which are characterized by I/S R3 with 85–90 % illite. Some samples collected at the bottom of the succession are characterized by the presence of lower amounts of I/S R0 with 30–50 % of illite associated with I/S R1.

6. SEM observations

The SEM images of selected mudrock samples show tiny glass shards that contain many vesicles similar to pumice. Some vesicles are oval and others are stretched into long, thin 'capillary' tubes (Fig. 6a–d). The smectite lattice, the mineral precursor to the

Table 4. Mineralogical features of the mudrock < 2 μm fraction

						I/S features % illite		
Sample	Kao	Chl	C/S	Ill	I/S	R0	R1	R3
FP123	tr	3	tr	7	89	n.d.	70–75	n.d.
FP124	tr	8	1	16	75	n.d.	65–75	n.d.
FP125	1	2	tr	5	91	30–40	65–70	n.d.
FP126	5	4	0	18	73	30–40	65	n.d.
FP127	0	2	0	8	90	35–40	65–70	n.d.
FP128	4	2	1	12	81	35–40	65–70	n.d.
FP129	tr	5	1	10	84	45–50	70	n.d.
FP130	tr	1	0	3	95	45–50	70–75	n.d.
FP131	tr	4	1	9	85	n.d.	80–85	n.d.
FP132	tr	4	1	8	88	n.d.	75	88–90
FP133	0	1	tr	3	95	n.d.	75	88–90
FP134	0	5	2	10	83	n.d.	70–75	88–90
FP135	tr	2	0	4	94	n.d.	82–85	n.d.
FP136	0	3	1	5	91	n.d.	82–85	n.d.
FP137	2	5	0	14	80	n.d.	n.d.	85–90
FP138	0	1	tr	3	96	n.d.	n.d.	85
FP139	0	1	1	2	96	n.d.	82–85	n.d.
FP140	tr	4	3	9	83	n.d.	n.d.	85

I/S – illite/smectite mixed layers; Ill – illite; C/S – chlorite/smectite mixed layers; Kao – kaolinite; Chl – chlorite; tr – trace; n.d. – not detected; R – Reichweite (stacking order of the illite/smectite (I/S) mixed layer).

(diagenetic) interstratified I/S identified in the studied samples, is commonly derived from the weathering of volcanic glass shards (e.g. Andreozzi, Dinelli & Tateo, 1997; Fesneau *et al*. 2009 and references therein). Thus, the abundance of smectite layers in the I/S mixed layers is probably related to the alteration of pyroclastic and/or volcaniclastic rocks. Diagenetic alteration of volcanic glass shards may characterize the source for the smectite and thus for interstratified I/S layers. Many studies have shown that the shard remnants are substituted by clay minerals and quartz, or rarely by calcite (Andreozzi *et al*. 1997).

https://doi.org/10.1017/S001675681100094X Published online by Cambridge University Press

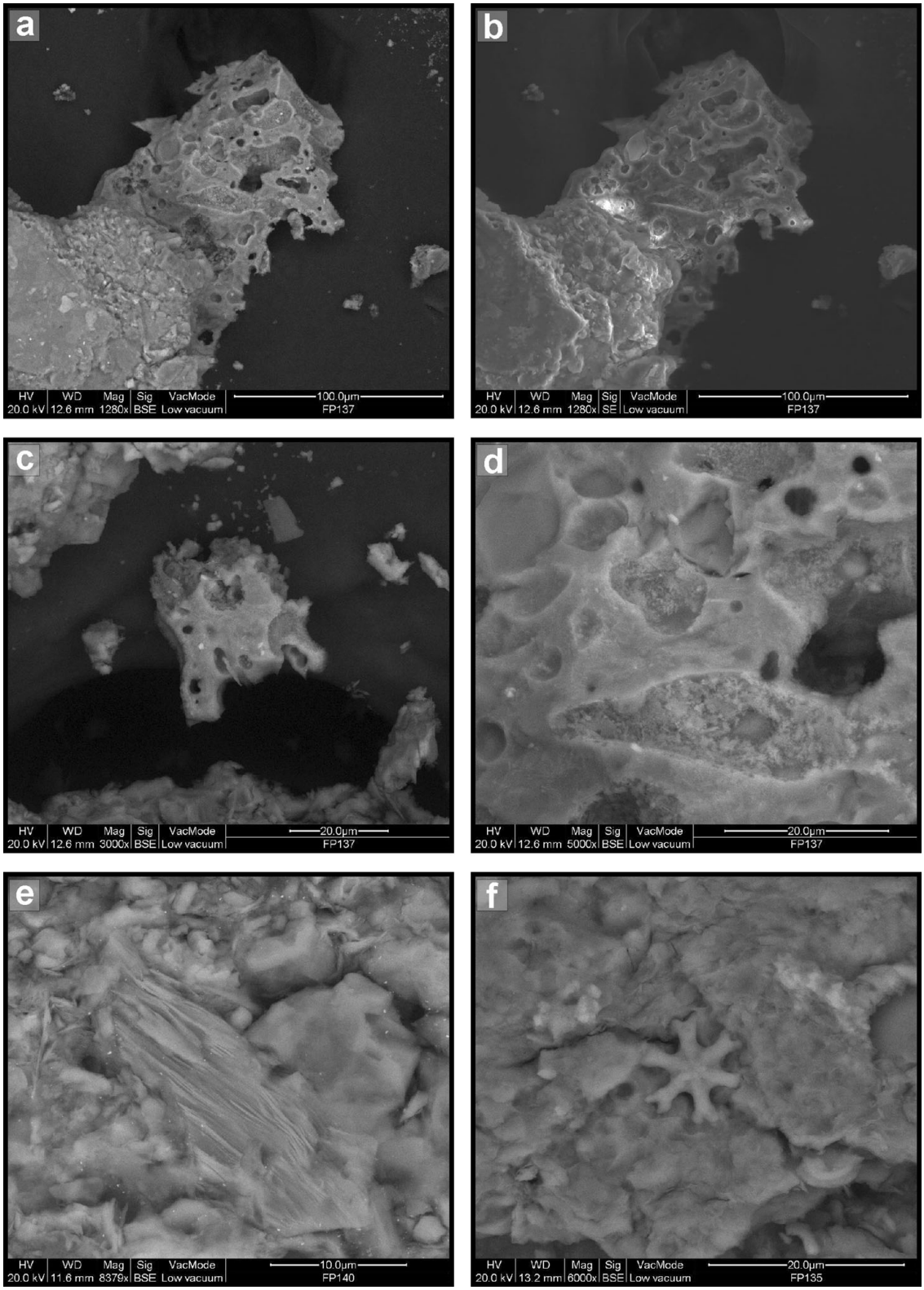

Figure 6. SEM (scanning electron microscope) images of mudrock samples. (a–d) Volcanic glass shards containing many vesicles. (e) Phyllosilicates and quartz grains. (f) Thin clay coating and microfossils.

7. Whole-rock geochemistry

7.a. Major element geochemistry

The elemental concentrations and some selected elemental ratios obtained from the studied mudrocks are given in Table 5. Figure 7 shows the major and trace elemental distributions normalized to Upper Continental Crust (UCC) averages (McLennan, Taylor & Hemming, 2006; diagram after Floyd, Winchester & Park, 1989).

The studied samples are characterized by narrow compositional changes for Al_2O_3, Fe_2O_3, and K_2O, which have concentrations close to those of UCC (McLennan, Taylor & Hemming, 2006). MgO and TiO_2

https://doi.org/10.1017/S001675681100094X Published online by Cambridge University Press

Table 5. Major, trace element and ratios distribution in mudrock samples

Sample	FP123	FP124	FP125	FP126	FP127	FP128	FP129	FP130	FP131	FP132	FP133	FP134	FP135	FP136	FP137	FP138	FP139	FP140
Oxides (wt%)																		
SiO_2	36.42	43.60	41.94	42.95	36.22	44.53	51.60	46.16	51.18	52.24	49.55	54.26	50.63	47.46	48.07	53.74	48.99	55.45
TiO_2	0.62	0.62	0.88	0.77	0.77	0.88	0.71	0.70	0.64	0.70	0.75	0.69	0.80	0.69	0.63	0.75	0.72	0.68
Al_2O_3	11.57	12.45	13.47	14.75	10.57	16.55	15.88	13.95	12.74	15.57	15.62	14.83	15.77	14.30	14.61	16.34	13.61	15.77
Fe_2O_3	3.00	4.23	3.92	4.39	3.61	4.41	6.47	4.92	4.49	6.69	5.22	6.31	6.61	6.19	7.07	7.12	5.51	6.78
MnO	0.09	0.08	0.03	0.04	0.10	0.04	0.04	0.02	0.05	0.04	0.02	0.05	0.04	0.04	0.06	0.06	0.07	0.06
MgO	3.00	3.49	3.64	3.41	2.98	3.47	4.42	4.06	3.85	4.54	4.38	4.19	4.46	4.30	4.72	4.43	3.89	4.43
CaO	17.42	14.39	11.58	10.89	16.67	7.18	4.98	7.02	9.50	3.74	4.32	5.61	4.16	5.43	3.60	1.61	7.64	2.89
Na_2O	0.02	0.32	0.01	0.02	0.01	0.00	0.82	0.03	0.48	0.43	0.10	1.70	0.70	0.12	1.67	0.42	0.18	0.79
K_2O	3.07	2.56	3.00	3.00	3.00	3.37	2.96	3.61	2.93	3.80	4.50	2.53	3.99	4.42	3.04	4.88	4.11	3.93
P_2O_5	0.13	0.09	0.11	0.12	0.13	0.10	0.09	0.11	0.08	0.08	0.10	0.12	0.10	0.11	0.11	0.08	0.10	0.08
LOI	24.17	17.85	21.22	19.14	25.13	19.16	11.20	19.19	13.84	11.91	15.13	9.19	12.51	16.82	15.68	10.15	14.19	8.51
Tot	99.49	99.67	99.78	99.48	99.18	99.69	99.18	99.78	99.78	99.73	99.69	99.48	99.78	99.87	99.25	99.58	99.01	99.37
Trace elements (ppm)																		
V	153.00	156.00	159.00	185.00	137.00	216.00	161.00	186.00	177.00	172.00	204.00	145.00	184.00	182.00	192.00	193.00	189.00	181.00
Cu	36.04	36.83	30.49	29.59	27.68	25.48	36.57	25.57	21.75	43.06	24.27	27.48	51.33	35.89	33.54	36.66	28.95	58.68
Co	10.00	13.00	15.00	12.00	12.00	25.00	13.00	10.00	14.00	17.00	14.00	21.00	19.00	21.00	12.00	12.00	15.00	19.00
Cr	104.00	120.00	128.00	144.00	113.00	159.00	139.00	144.00	140.00	151.00	149.00	92.00	140.00	144.00	116.00	139.00	143.00	172.00
Ni	58.24	90.45	61.76	57.67	39.04	115.65	100.24	53.13	83.24	95.50	65.97	101.12	76.86	83.52	59.17	63.84	66.18	118.73
Sc	13.20	13.80	14.10	15.10	11.50	16.70	16.70	14.00	14.10	16.70	16.00	14.90	16.50	15.70	16.40	16.70	15.00	16.10
Zn	100.00	150.00	140.00	110.00	140.00	120.00	180.00	120.00	130.00	150.00	120.00	140.00	160.00	140.00	160.00	160.00	130.00	140.00
Cs	9.00	8.70	10.50	11.40	11.30	12.40	10.20	14.00	13.60	16.40	15.60	7.20	15.30	17.00	9.30	19.60	17.20	14.60
Sr	658.00	520.00	699.00	619.00	655.00	390.00	337.00	458.00	372.00	286.00	285.00	397.00	305.00	265.00	293.00	250.00	344.00	230.00
Ba	170.00	250.00	170.00	190.00	230.00	150.00	420.00	250.00	260.00	290.00	320.00	320.00	330.00	340.00	390.00	290.00	250.00	340.00
Rb	120.00	110.00	140.00	130.00	140.00	170.00	150.00	170.00	150.00	190.00	210.00	100.00	190.00	200.00	130.00	250.00	210.00	200.00
Y	39.00	21.00	31.00	27.00	37.00	27.00	18.00	22.00	21.00	19.00	24.00	18.00	23.00	23.00	22.00	20.00	25.00	20.00
Zr	127.00	131.00	198.00	155.00	174.00	175.00	157.00	146.00	131.00	138.00	169.00	166.00	189.00	130.00	154.00	153.00	153.00	141.00
Nb	12.00	11.00	25.00	18.00	23.00	23.00	15.00	18.00	13.00	17.00	23.00	13.00	26.00	16.00	15.00	20.00	17.00	15.00
Hf	3.20	3.80	5.00	3.60	4.70	4.10	4.90	3.70	3.50	4.10	4.40	4.90	5.10	3.60	4.70	4.30	4.60	4.30
Th	6.80	9.30	9.70	9.20	7.90	10.60	13.00	8.80	8.60	11.10	9.70	12.70	12.10	10.10	13.00	10.40	9.70	11.70
U	2.30	3.20	2.60	1.80	2.10	1.80	4.20	2.10	2.70	2.50	2.70	4.20	4.00	2.70	4.20	2.90	2.50	2.70
La	36.20	25.00	43.30	36.80	36.80	48.10	26.20	28.40	18.70	27.70	17.90	31.80	25.30	30.40	31.00	32.40	29.20	22.90
Ce	70.00	52.00	79.00	71.00	64.00	93.00	55.00	57.00	43.00	58.00	49.00	61.00	55.00	64.00	55.00	61.00	63.00	52.00
Nd	30.00	20.00	38.00	29.00	20.00	39.00	22.00	25.00	17.00	26.00	29.00	21.00	22.00	22.00	20.00	17.00	22.00	15.00
Sm	5.70	3.80	6.10	5.60	5.40	5.90	3.90	5.00	4.20	4.80	5.60	4.20	5.80	5.90	5.00	5.20	5.70	4.80
Eu	1.40	0.90	1.50	1.40	1.30	1.20	0.80	1.20	1.00	1.10	1.40	0.90	1.40	1.30	1.00	1.20	1.30	1.00
Tb	0.80	0.50	0.70	0.80	0.50	0.50	0.50	0.60	0.50	0.60	0.60	0.50	0.80	0.80	0.50	0.80	0.90	0.50
Yb	2.50	2.30	2.50	2.20	2.20	2.90	2.40	2.20	2.40	2.40	2.80	2.00	2.80	2.50	2.30	2.30	2.60	2.80
Lu	0.32	0.30	0.32	0.28	0.40	0.34	0.33	0.29	0.32	0.31	0.36	0.27	0.50	0.41	0.42	0.39	0.49	0.53
Ratios																		
CIA	67.06	69.21	69.66	71.74	67.32	71.64	71.05	68.65	65.22	66.31	64.62	65.29	66.59	64.51	65.31	64.92	65.30	65.91
Eu/Eu^*	0.78	0.99	0.82	0.79	1.03	0.88	0.86	0.79	0.78	0.75	0.84	0.90	0.77	0.70	0.85	0.71	0.70	0.89
K/Cs	3406	2938	2859	2633	2655	2718	2904	2579	2157	2315	2882	3513	2610	2599	3264	2490	2391	2691
Zr/Ti	0.02	0.02	0.02	0.02	0.02	0.02	0.02	0.02	0.02	0.02	0.02	0.02	0.02	0.02	0.02	0.02	0.02	0.02
Nb/Y	0.31	0.52	0.81	0.67	0.62	0.85	0.83	0.82	0.62	0.89	0.96	0.72	1.13	0.70	0.68	1.00	0.68	0.75
Zr/Sc	9.62	9.49	14.04	10.26	15.13	10.48	9.40	10.43	9.29	8.26	10.56	11.14	11.45	8.28	9.39	9.16	10.20	8.76
Th/Sc	0.52	0.67	0.69	0.61	0.69	0.63	0.78	0.63	0.61	0.66	0.61	0.85	0.73	0.64	0.79	0.62	0.65	0.73
Cr/V	0.68	0.77	0.81	0.78	0.82	0.74	0.86	0.77	0.79	0.88	0.73	0.63	0.76	0.79	0.60	0.72	0.76	0.95
Y/Ni	0.67	0.23	0.50	0.47	0.95	0.23	0.18	0.41	0.25	0.20	0.36	0.18	0.30	0.28	0.37	0.31	0.38	0.17
Cr/Th	15.29	12.90	13.20	15.65	14.30	15.00	10.69	16.36	16.28	13.60	15.36	7.24	11.57	14.26	8.92	13.37	14.74	14.70
Th/Sc	0.52	0.67	0.69	0.61	0.69	0.63	0.78	0.63	0.61	0.66	0.61	0.85	0.73	0.64	0.79	0.62	0.65	0.73

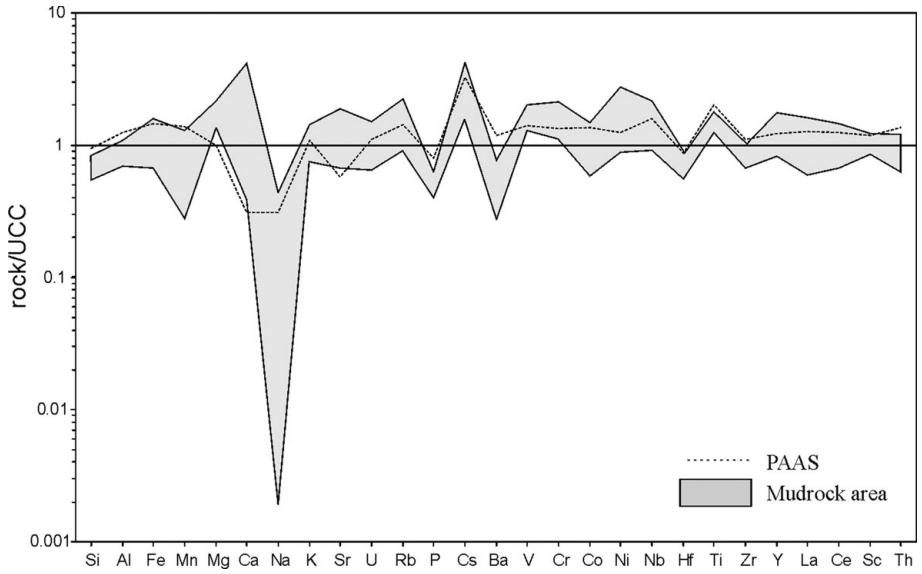

Figure 7. Major and trace element compositions of Tufiti di Tusa mudrocks normalized to average Upper Continental Crust (UCC) (McLennan, Taylor & Hemming, 2006; diagram after Floyd, Winchester & Park, 1989). The composition of Post-Archaean Australian Shales (PAAS; Taylor & McLennan, 1985) is shown for comparison.

show a moderate enrichment (Fig. 7). MgO enrichment may be related to the 2:1 expandable clay minerals (e.g. smectite). CaO is the most enriched oxide compared to UCC, and shows highly variable concentrations ranging from 1.61 to 17.42 wt %. MnO is also variable, with concentrations ranging from 0.02 to 0.10 wt %. SiO_2, P_2O_5 and Na_2O are strongly depleted relative to UCC (Fig. 7). High variations in Na_2O concentrations are related to plagioclase contents. These variations may reflect an andesitic volcanic arc input, as testified by the petrographical signature (e.g. abundant plagioclase in petrofacies B–C–D).

Most oxides (Al_2O_3, SiO_2, Fe_2O_3, MgO, Na_2O and K_2O) are positively correlated whereas CaO is negatively correlated with the other oxides, reflecting variations in the carbonate component. Mobile and immobile element oxides (e.g. Al_2O_3, CaO, Na_2O and K_2O) have been used as a proxy for chemical weathering in sediment source areas, on the basis of the chemical index of alteration ($CIA = 100^*(Al_2O_3/(Al_2O_3 + CaO^* + Na_2O + K_2O))$) (Nesbitt & Young, 1982). The CaO^* values used are related exclusively to the silicate fraction (thus excluding the CaO related to the carbonate and sulphate minerals calculated via XRD). The Tufiti di Tusa mudrocks have CIA values ranging from 63.20 to 71.64 (average = 66.55 ± 2.89).

7.b. Trace element composition and rare earth elements

Strontium, like calcium, is enriched relative to UCC. Rubidium is also enriched and shows a significant correlation with K (r = 0.93) suggesting these elements are mostly controlled by the mica-like clay minerals.

High-field-strength trace elements (HFSE) have concentrations similar to those of UCC (Fig. 7). The lack of correlation between HFSE and Al_2O_3 is consistent with these elements being generally contained in accessory phases in mudrocks (e.g. Slack & Stevens, 1994). We infer that these elements occur in the sediment mostly as resistate phases, supporting the idea that they efficiently record the provenance (McLennan, Hemming & Hanson, 1993 and many others). Concentrations of the transition elements (Cr, Co, Ni and V) are generally higher than in UCC. All the transition metals appear to covary positively with Al_2O_3 and Fe_2O_3 suggesting these trace elements are mostly hosted by mica-like clay minerals.

Trace metals V, Mn, Cr, Zn and U can be used to trace an anoxic environment in which these elements are enriched (e.g. Bertolino, Zimmerman & Sattler, 2007 and references therein). U is relatively unstable under oxidizing conditions but much more stable in anoxic environments (McLennan, Hemming & Hanson, 1993). Generally, high U/Th ratios point to an anoxic depositional environment where U can be enriched. The studied mudrocks have low U/Th ratios (average = 0.28 ± 0.05), similar to the PAAS (Post-Archaean Australian Shales) (0.21) and UCC (0.26) values, typical of oxidizing environments.

The REEs have been normalized to PAAS (Taylor & McLennan, 1985); they display a pattern similar to the PAAS (Fig. 8). Most samples show a moderate depletion for both LREEs and HREEs, likely owing to a dilution effect exerted by the detrital carbonate component, which furnishes negligible REEs (e.g. Stevenson, Whittaker & Mountjoy, 2000), and a positive Eu anomaly possibly related to the feldspar content with respect to the PAAS standard, as also evident in mineralogical analyses.

8. Discussion

8.a. Provenance of the detrital material

The sandstone samples show abundant microlitic, felsitic seriate and vitric volcanic lithic fragments,

https://doi.org/10.1017/S001675681100094X Published online by Cambridge University Press

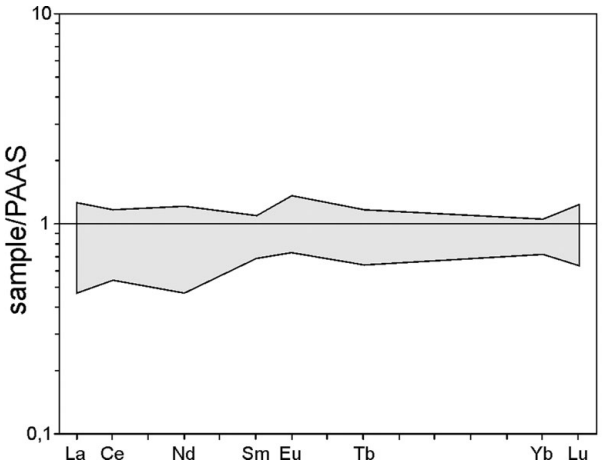

Figure 8. Rare earth element compositions of Tufiti di Tusa mudrocks normalized to Post-Archean Australian Shales (PAAS) (Taylor & McLennan, 1985).

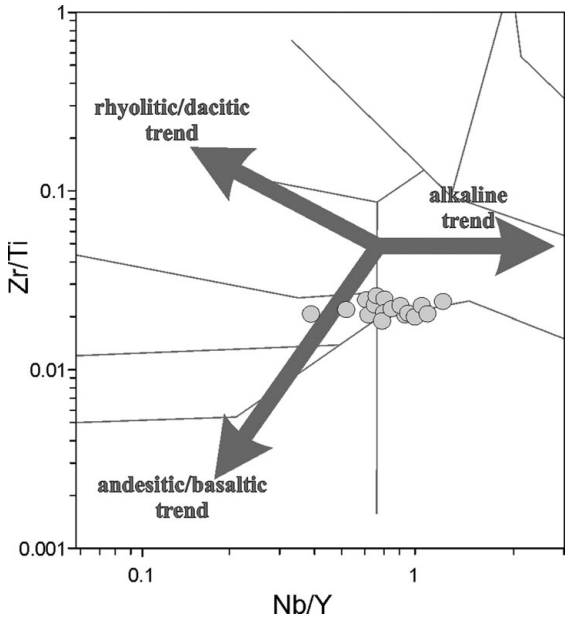

Figure 9. Nb/Y v. Zr/Ti plot (after Winchester & Floyd, 1977; Zimmermann & Spalletti, 2009) for the studied mudrocks, to reveal differences in the whole-rock composition of the studied mudrock samples.

with low-grade metamorphic fragments of phyllite, slate and quartzite, and intrabasinal and extrabasinal carbonate grains. The importance of the volcaniclastic supply is also testified by volcanic glass shards found in mudrocks. SEM images show tiny glass shards, consisting of many gas-bubble holes. The smectite lattice is commonly derived from the weathering of volcanic glass shards (Andreozzi, Dinelli & Tateo, 1997; Fesneau *et al*. 2009). Since the studied mudrocks contain abundant interstratified I/S, characterized also by R0 values with a high percentage of smectite in I/S mixed layers, the volcanic glass shards and, thus, the volcaniclastic input may play an important role in the sedimentary evolution of the studied succession.

The more immobile chemical elements, including Zr, Ti, Y and Nb, are generally used to determine the initial composition of the volcanic ashes and the type of magma (e.g. Winchester & Floyd, 1977; Zimmermann & Spalletti, 2009). The compositional trend of sedimentary rocks can be estimated by considering ratios of Nb/Y and Zr/Ti, recently used for clastic sediments (e.g. Fralick, 2003). In the Nb/Y versus Zr/Ti plot (Winchester & Floyd, 1977), the mudrock samples point to a mainly andesitic and trachy-andesitic composition, close to the alkaline and the andesitic/basaltic trend, partly caused by the relative depletion of Zr in relation to UCC, which consequently lowers the Zr/Ti ratio (Fig. 9). However, high Nb concentrations shift the Nb/Y ratios to an alkaline composition. Basic source terranes would have high ferromagnesian mineral abundances, resulting in high Cr/V ratios (> 8) and low Y/Ni (< 0.5). The studied mudrocks are characterized by a lower Cr/V ratio suggesting a minor basic input. The minor importance of a mafic supply is confirmed also by the La–Th–Sc ternary plot (Fig. 10). The mudrocks fall in a region close to the PAAS point, between the granite and andesite fields (Fig. 10), indicating intermediate-felsic compositions of the source areas. However, based on trace element contents (see the transition element contents in Table 5), a mixed source, characterized by intermediate-felsic rocks with minor mafic input, cannot be excluded. Both Cr/Th and Th/Sc ratios are considered robust provenance indicators (Floyd & Leveridge, 1987; Taylor & McLennan, 1985; McLennan, Hemming & Hanson, 1993). The diagram based on Cr/Th v. Th/Sc ratios (Fig. 11) shows that the mudrocks are consistent with mixing between felsic and mafic end-members, with a major contribution from an intermediate-felsic source; the mafic input is lower but not negligible.

The relative abundances of trace elements such as La and Th (indicative of a felsic igneous source) and Co, Cr and Sc (indicative of mafic sources) and ratios such as La/Sc, Th/Sc, Th/Cr, Cr/Th and Eu/Eu* were used to differentiate the source of sediments (e.g. Cullers, 2000; Roser *et al*. 2002). These ratios allow assessment of aspects of bulk source composition because they are resistant to alteration processes and, apart from the effects of dense mineral concentration, they may be only slightly modified during transport (Roser *et al*. 2002). The studied sediments show ratios similar to the PAAS and UCC and generally fall in the range of similar published data (e.g. Cullers, 2000), suggesting provenance from intermediate-felsic sources (Table 6).

Starting from these considerations, based on the sandstone petrography and the mineralogical-geochemical data of the associated mudrocks, we suggest that the Tufiti di Tusa Formation contains clastic contributions from different sources: (a) a terrigenous (siliciclastic) source mainly from metasedimentary and magmatic sources (Calabrian Palaeozoic and related magmatites), with minor, but not negligible mafic rock supply; (b) a volcaniclastic source from subduction-related andesites, probably located in Sardinia; and (c) a calciclastic source, probably derived from the Apenninic forebulge.

https://doi.org/10.1017/S001675681100094X Published online by Cambridge University Press

Table 6. Range of elemental ratios of mudrock samples compared to the ratios of felsic and mafic rocks, Upper Continental Crust and Post-Archaean Australian Shales

Elemental ratio	Range of the studied mudrock	Range of sediments[1]		Upper Continental Crust[2]	Post-Archaean Australian average shale[3]
		Felsic rocks	Mafic rocks		
Eu/Eu*	0.82 ± 0.09	0.32–0.83	0.70–1.02	0.65	0.66
La/Sc	2.04 ± 0.61	2.5–16.3	0.43–0.86	2.21	2.4
Th/Sc	0.67 ± 0.08	0.84–20.5	0.05–0.22	0.79	0.9
Th/Co	0.70 ± 0.16	0.67–19.4	0.04–1.4	0.63	0.63
Th/Cr	0.08 ± 0.02	0.13–2.7	0.43–0.86	2.21	2.4
Cr/Th	13.52 ± 2.49	4.00–15	25–500	7.76	7.53

[1]Cullers (2000); [2]McLennan *et al*. (2006); [3]Taylor & McLennan (1985).

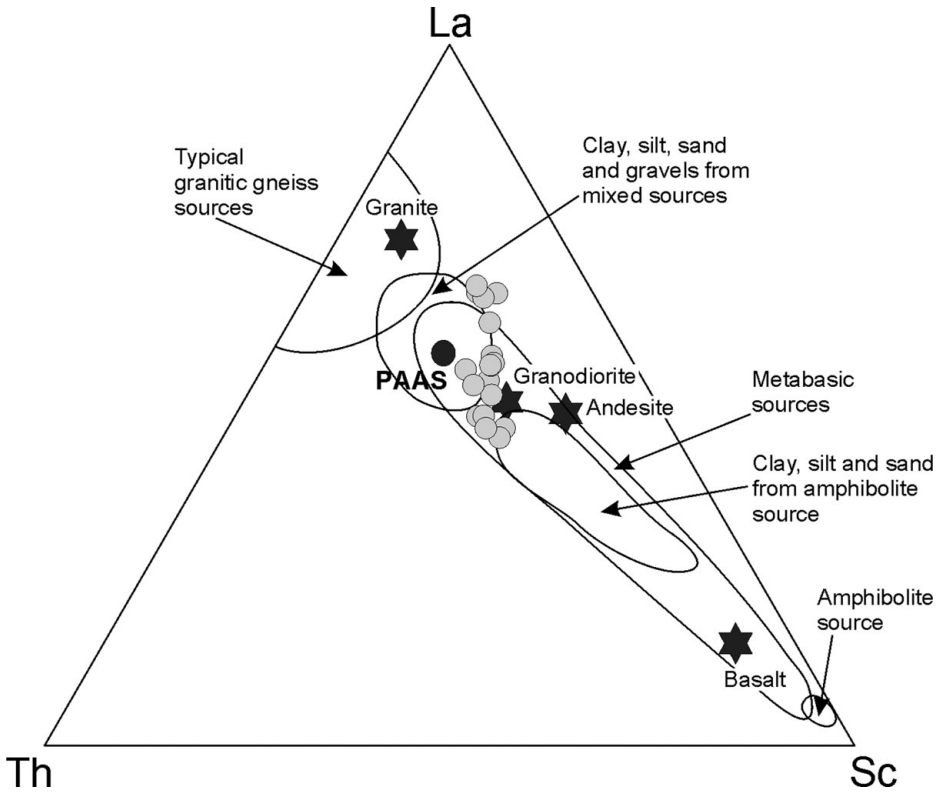

Figure 10. La–Th–Sc plot (Bhatia & Crook, 1986) for Tufiti di Tusa mudrocks. The mudrocks fall in a region close to PAAS that rules out important mafic supply.

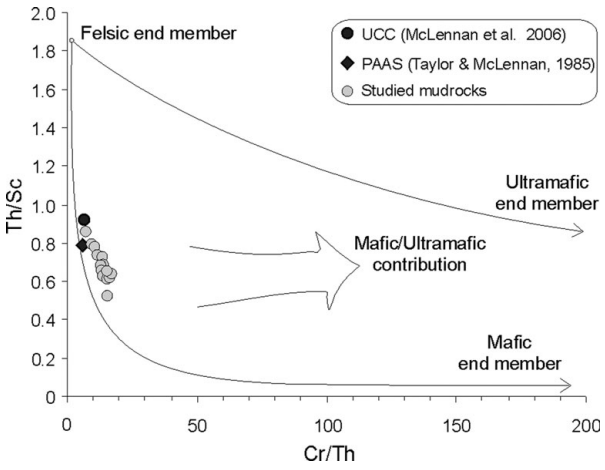

Figure 11. Cr/Th v. Th/Sc plot (Condie & Wronkiewicz, 1990) for Tufiti di Tusa mudrocks. Two mixing curves have been shown between a felsic end-member and mafic and ultramafic end-members.

8.b. Diagenetic grade

There is a broad consensus in the literature about the hypothesis that smectite-to-illite conversion is a progressive trend mainly controlled by temperature (e.g. Merriman & Peacor, 1999). Furthermore, this process may be influenced by time, and K-availability, whose origin has been assigned to feldspars and/or mica (e.g. Moore & Reynolds, 1997; Cavalcante *et al*. 2007).

The abundance of I–S R1 mixed layers in the studied samples suggests that the Tufiti di Tusa Formation was affected by medium diagenetic grade (Merriman & Peacor, 1999 and references therein). These conditions are equivalent to those found in Sicilide successions located to the northwest of the studied area (Cavalcante *et al*. 2007).

The upper part of the studied succession is characterized by samples showing I/S R3 with higher illite amounts and a higher concentration of feldspars and K_2O (Tables 3, 5). This suggests that the illitization

https://doi.org/10.1017/S001675681100094X Published online by Cambridge University Press

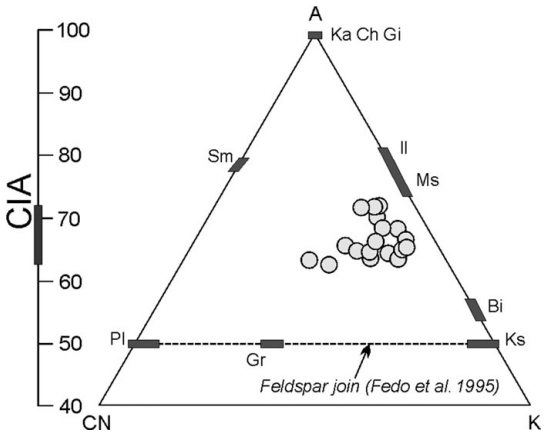

Figure 12. A–CN–K diagram (in molecular proportions) for mudrock samples (Nesbitt & Young, 1982). Note only the top 60 % of the triangle is shown. Legend: A – Al_2O_3; C – CaO; N – Na_2O; K – K_2O; Gr – granite; Ms – muscovite; Il – illite; Ka – kaolinite; Ch – chlorite; Gi – gibbsite; Sm – smectite; Bi – biotite; Ks – K-feldspar; Pl – plagioclase.

of smectite is influenced by K-availability, as most models have proposed to explain the smectite-to-illite transformation (e.g. Moore & Reynolds, 1997; Cavalcante *et al*. 2007).

8.c. Source-area weathering, recycling and sorting

Various indices of weathering have been proposed based on different molecular proportions of mobile element oxides (Na_2O, CaO, MgO, K_2O) relative to immobile element oxides, Al_2O_3, ZrO, and Ti_2O. The CIA has been widely used as a proxy for chemical weathering in the sediment source area. The Al_2O_3, Na_2O and K_2O values, and the CaO^* belonging exclusively to the silicate fraction, have been plotted in the A–CN–K triangular diagram (Fig. 12). The Tufiti di Tusa mudrocks form a tight group above the A_{50} line (the feldspar join; Fedo, Nesbitt & Young, 1995) with a vector parallel to the CN–A join and a vector parallel on the A–K join, close to the illite–muscovite point (Fig. 12). Illite and other illitic minerals (I/S mixed layers) are the dominant clay minerals that characterize the studied samples. The degree of weathering is variable within the individual suites. The variations of CIA values along the stratigraphic section are related to the mineralogical variations. The samples with higher CIA values (lower part of the succession) are characterized by abundant phyllosilicates and minor content of feldspars, whereas the samples with lower CIA values show lower percentages of phyllosilicates and higher contents of feldspars. This feature emphasizes the coherent nature of the mineralogical transformation (from primary feldspars to secondary clay minerals) that are clearly related to the CIA value distribution.

Likewise, the degree of chemical weathering can be assessed on the basis of K/Cs ratios in fine-grained sedimentary rocks (e.g. McLennan, Hemming & Hanson, 1993). Caesium is enriched in clay minerals during weathering, which leads to a decrease in K/Cs ratios of the rocks with increasing weathering. Correlation between K and Cs ($r = 0.85$) is strongly indicative of weathering affecting K-bearing minerals (e.g. Feng & Kerrich, 1990). The studied samples show K/Cs values ranging from 2200 to 3400 (average = 2800), which are similar to the PAAS value (2100), testifying to a moderate weathering in the source area. At the same time, source area weathering can be evaluated by clayeyness (Al/Si ratio), which increases owing to clay production during pedogenesis (e.g. Mitchell & Sheldon, 2009 and references therein). The Tufiti di Tusa sediments show an average Al/Si ratio (0.34 ± 0.03) close to the PAAS and UCC averages (respectively, 0.34 and 0.26; Taylor & McLennan, 1985; McLennan, Taylor & Hemming, 2006). This suggests that the degree of source-area weathering was most probably moderate rather than intense.

One approach to estimate the amount of primary source relative to weathered minerals in shales and siltstones is to use the index of compositional variability (ICV = $(Fe_2O_3 + K_2O + Na_2O + CaO + MgO + TiO_2)/Al_2O_3$) (Cox & Lowe, 1995); in this equation, CaO includes also the Ca-sources related to detrital carbonate and phosphate (e.g. LaMaskin, Dorsey & Vervoort, 2008). The ICV values tend to be highest for detrital ferromagnesian minerals and feldspars and lowest for minerals that form during weathering (clay minerals). Thus, the ICV values for siltstones and shales with abundant relatively unweathered detrital minerals should be greater than one. In contrast, siltstones and shales composed of abundant clay minerals have an ICV less than one. Most terrigenous sedimentary rocks with ICV values greater than one tend to occur in first-cycle deposits, whereas sedimentary rocks with ICV values less than one usually form where intense weathering and minimal tectonic uplift have occurred (Cox & Lowe, 1995). Some first-cycle shales and siltstones formed during intense chemical weathering may form, however, abundant clay minerals and thus contain ICV values less than one (Johnsson, 2000). The ICV values of the studied samples are more than one (average ICV = 1.6) and, consequently, they indicate input of first-cycle sediments without important recycling processes.

Generally, mature sediments consisting of both sandstones and shales show a wide range of TiO_2/Zr variations whereas immature sediments show a more limited range of TiO_2/Zr variations in the Al–Ti–Zr ternary diagram (Garcia *et al*. 1994). The studied sediments are confined to the centre of this diagram, with a limited range of TiO_2/Zr variations, suggesting poor sorting and rapid deposition of the sediments (Fig. 13).

The sedimentary sorting and recycling can be further monitored by a plot of Th/Sc against Zr/Sc (McLennan, Hemming & Hanson, 1993); as the studied mudrocks are not recycled sedimentary rocks, the samples plot along the simple positive correlation between these ratios (i.e. Th/Sc v. Zr/Sc). The studied sediments follow a general trend consistent with their direct

https://doi.org/10.1017/S001675681100094X Published online by Cambridge University Press

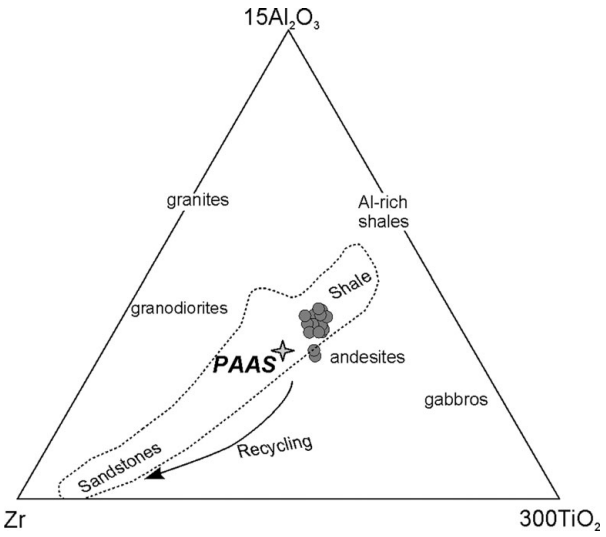

Figure 13. Ternary $15Al_2O_3$–$300TiO_2$–Zr plot (after Garcia, Fonteilles & Moutte, 1994) for Tufiti di Tusa mudrocks, showing poor sorting and rapid deposition of the sediments.

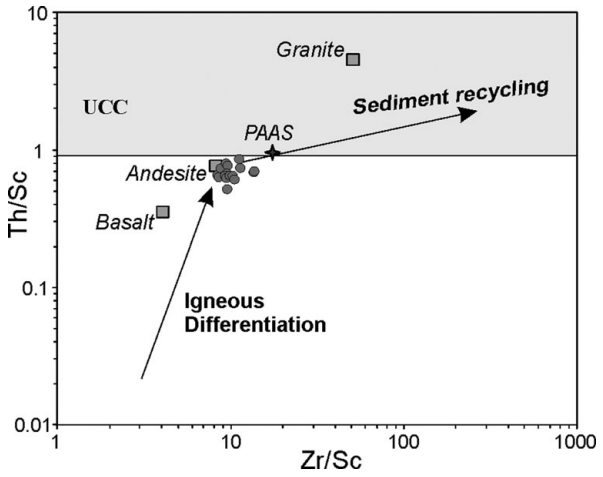

Figure 14. Th/Sc v. Zr/Sc plot (McLennan, Hemming & Hanson, 1993) for Tufiti di Tusa mudrocks. Studied mudrocks fall close to the andesite composition.

derivation from igneous rocks in the Th/Sc v. Zr/Sc diagram (Fig. 14). This consideration is in agreement with the ICV values and the Al–Ti–Zr diagram constraints.

Commonly, recycling processes are related to the amount of feldspars in the sediments; the paucity or absence of feldspars in the rocks may record a recycling effect (Mongelli *et al*. 2006; Perri *et al*. 2008, 2010; Zaghloul *et al*. 2010). Many of the studied samples are characterized by significant amounts of plagioclase feldspars; this testifies to poor recycling effect for the studied sediments. Plagioclases are abundant in sandstone; they are fresh and dominantly derived from active volcanic source areas, testifying to poor recycling and low–moderate weathering.

8.d. Geodynamic and palaeogeographic significance

The compositional variations recorded in the studied succession, as shown above, are related to palaeogeographic and geodynamic change during early Miocene time (Fig. 15).

In the southern Italy domain, the Sicilide Complex strata represent deposition in a remnant ocean basin related to the western subduction of the Adria oceanic lithosphere beneath the Iberia plate (e.g. Guerrera, Martín-Algarra & Perrone, 1993; Critelli & Le Pera, 1998; Critelli, 1999). The subduction was active for all the Palaeogene and early Miocene, producing an accretionary prism, the Sicilide Complex and calcalkaline volcanism in Sardinia. The Mesoalpine (Eocene to early Oligocene) tectonic phase in southern Italy corresponds to the subduction of the Adria–Ionian oceanic lithosphere beneath the Iberian plate. During early to middle Miocene time, the Apenninic domain is the place where an immense volume of turbiditic sedimentation is a response to E–NE accretionary processes along the Adria plate (e.g. Patacca & Scandone, 2007 and references therein).

The Tufiti di Tusa Formation, representing the first foredeep deposit within the southern Apennine orogenic belt, records interbedded provenances from the (i) Fold–Thrust Belt (quartzolithic petrofacies), where metamorphic, plutonic and extrabasinal carbonate detritus are derived from the internal units of the growing orogen, that in the southern Italy orogenic system correspond to the Calabria–Peloritani Terrane and the Longobucco Unit (Fig. 15), (ii) Forebulge Region (carbonatoclastic strata), where carbonate turbidites interbedded with siliciclastic turbidites are derived from the flexed forebulge depozones of the Adria margin (Fig. 15), and (iii) the active volcanic arc from Sardinia (volcaniclastic petrofacies). Huge quartzose supply (Numidian sandstones; Fig. 15), during the early stage of collision, is widespread along the Adria margin, representing key signatures from the cratonic provenance from the northern African continental margin (Fig. 15) that are partially coeval with deposition of the Tufiti di Tusa Formation, and accommodated in subsiding depozones of the Adria margin (e.g. Critelli, 1999 and references therein).

9. Conclusions

The studied succession from the Tufiti di Tusa Formation (Sicilide Complex, southern Italy) is characterized by an evolution from calcilcastic–siliciclastic sediments to mostly volcaniclastic sediments; both mudrock mineralogy and sandstone petrography show this trend. The lower part of the succession is characterized by sandstone quartzolithic beds (petrofacies A) and carbonate-rich mudrocks, whereas the mudrock and, mostly, the sandstone samples collected along the upper part show an increase in feldspar content (petrofacies D) related to volcanic arc provenance.

The mudrocks studied are mineralogically characterized by phyllosilicates, quartz, calcite and feldspars, with a small amount of gypsum detected in some samples. I/S mixed layers are the main phases among the phyllosilicates, followed by 10-Å minerals (illite

https://doi.org/10.1017/S001675681100094X Published online by Cambridge University Press

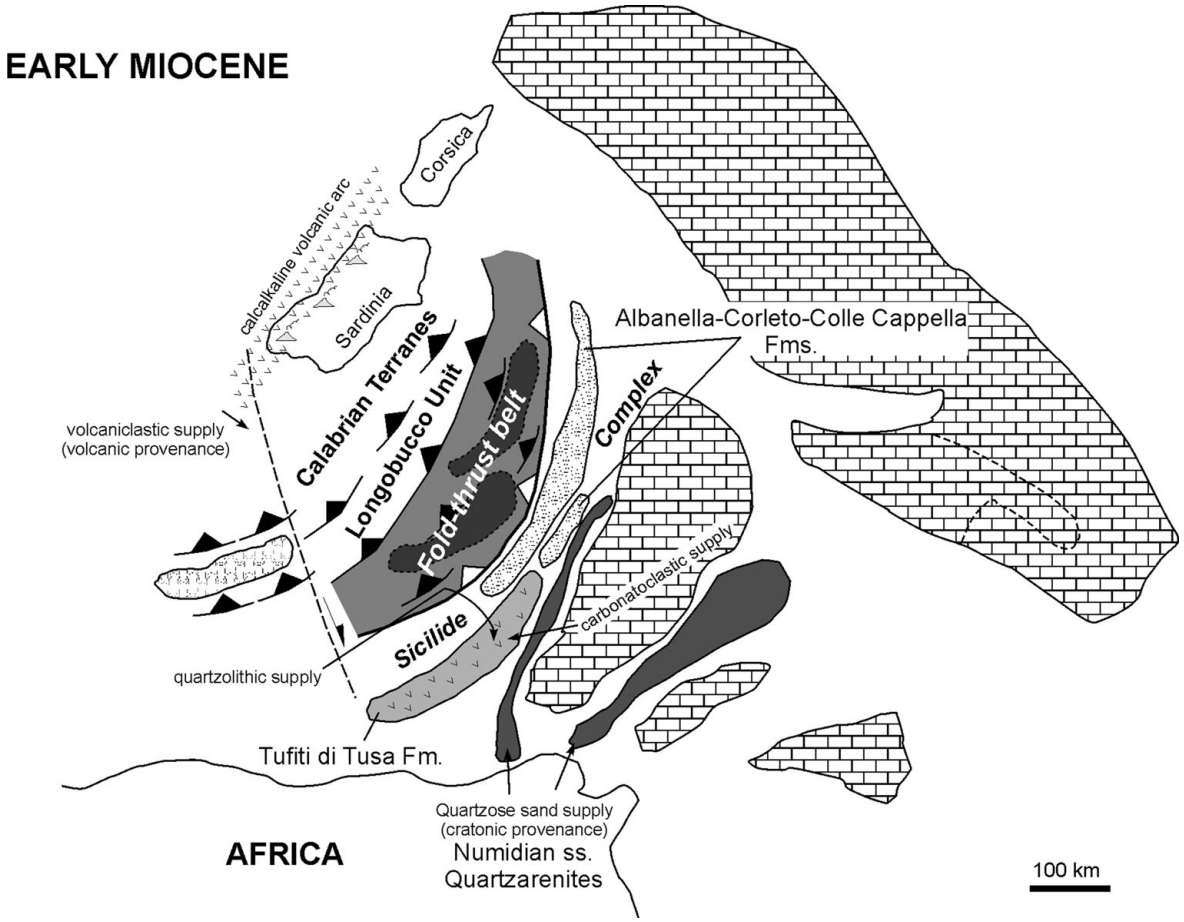

Figure 15. Palaeogeographic reconstructions (early Miocene) of the western Mediterranean during progressive closure of the remnant ocean basin and onset of collision in the southern Apennines (modified from Critelli, 1999).

and micas) and chlorite, while kaolinite and C/S mixed layers are present in a few per cent or trace amounts. The abundance of I/S R1 and R3 mixed layers suggest that the Tufiti di Tusa Formation has been affected by medium diagenetic grade. The upper part of the succession shows stronger illitization. This suggests an influence of K-availability on the smectite illitization.

The source-area weathering has been evaluated by the CIA index. The studied mudrocks are characterized by CIA values in the range 65–72, testifying to moderate weathering at the source areas. Furthermore, low K/Cs ratios of the studied sediments suggest that the weathering degree of the source area was moderate rather than intense. In general, warm climates favour an intense source-area weathering, and the formation of residual clays like kaolinite. The studied mudrocks are characterized by low kaolinite, which is only present in a few samples. Thus, weathering occurred under warm and episodically wet climates with a dry season (typical Mediterranean climate) that promoted rapid sedimentation without strong sedimentary recycling (e.g. Mongelli *et al*. 2006 and references therein). The high ICV values of the studied samples suggest that they are related to first-cycle material and not dominated by recycling. The distribution of the studied mudrocks in the Al–Ti–Zr ternary diagram and in the Th/Sc v. Zr/Sc plot also suggests poor sorting and rapid deposition of the sediments. The sandstone petrology confirms the poor sorting without significant recycling processes as shown by detrital grain features.

The source areas of the studied sediments are mainly characterized by metasediments (low-to-high grade metamorphic rocks) of the Palaeozoic basement with andesitic to felsic volcanic bodies. The limited importance of a mafic supply is confirmed by the Cr/V and Y/Ni ratios, by the K_2O v. Rb plot and by the La/Sc, Th/Sc, Th/Co, Th/Cr, Cr/Th and Eu/Eu* ratios, that suggest a provenance from source areas fairly intermediate–felsic rather than mafic in composition.

Direct evidence of volcaniclastic supply is shown by volcanic glass shards found in thin mudrock levels, and the abundance of smectite layers in the I/S mixed layers are probably related to the diagenetic alteration of the weathered original pyroclastic and/or volcaniclastic rocks, which were the source for the smectite, and thus for the interstratified I/S layers.

A large amount of volcanic detritus rapidly filled the basin; the volcaniclastic sedimentation gave rise either to fine-grained, small pure beds or, more frequently, to thick arenitic impure beds. According to the palaeogeographic and geodynamic settings, the volcanic ash-falls may originate at and be derived from the subduction-related orogenic volcanism of Sardinia,

https://doi.org/10.1017/S001675681100094X Published online by Cambridge University Press

characterized by andesitic–rhyolitc volcanic products during Oligocene–Miocene time.

Acknowledgements. This research has been carried out within the MIUR-ex60% Projects (Palaeogeographic and Palaeotectonic Evolution of the Circum-Mediterranean Orogenic Belts, 2001–2005; and Relationships between Tectonic Accretion, Volcanism and Clastic Sedimentation within the Circum-Mediterranean Orogenic Belts, 2006; Resp. S. Critelli) and the 2006–2008 MIUR-PRIN Project 2006.04.8397 ('The Cenozoic clastic sedimentation within the circum-Mediterranean orogenic belts: implications for palaeogeographic and palaeotectonic evolution'; Resp. S. Critelli). The authors are indebted to Agustín Martín-Algarra, two anonymous referees and the editor Phil Leat for their reviews and suggestions on an earlier version of the manuscript.

References

ANDREOZZI, M., DINELLI, E. & TATEO, F. 1997. Geochemical and mineralogical criteria for the identification of ash layers in the stratigraphic framework of a foredeep; the Early Miocene Mt. Cervarola Sandstones, Northern Italy. *Chemical Geology* **137**, 23–39.

ASSORGIA, A., BARCA, S., ONNIS, G., SECCHI, F. A. G. & SPANO, C. 1986. Episodi sedimentari e vulcanici nel settore occidentale dell'Arcuentu e loro contesto geodinamico (Sardegna SW). *Memorie della Società Geologica Italiana* **35**, 229–40.

BERTOLINO, S. R. L., ZIMMERMANN, U. & SATTLER, F. 2007. Mineralogy and geochemistry of bottom sediments from water reservoirs in the vicinity of Córdoba, Argentina: environmental and health constraints. *Applied Clay Science* **36**, 206–20.

BHATIA, M. R. & CROOK, K. A. W. 1986. Trace element characteristics of graywackes and tectonic setting discrimination of sedimentary basins. *Contributions to Mineralogy and Petrology* **92**, 181–93.

BONARDI, G., CAVAZZA, W., PERRONE, V. & ROSSI, S. 2001. Calabria-Peloritani Terrane and Northern Ionian Sea. In *Anatomy of an Orogen: The Apennines and Adjacent Mediterranean Basins* (eds G. B. Vai & I. P. Martini), pp. 287–306. Dordrecht: Kluwer Academic Publishers.

BONI, M., DEL VECCHIO, L. & LIRER, L. 1990. Considerazioni sul vulcanismo esplosivo miocenico della Sardegna S-W. *Memorie della Società Geologica Italiana* **45**, 989–1000.

CARACCIOLO, L., LE PERA, E., MUTO, F. & PERRI, F. 2009. Sandstone petrology and muddstone geochemistry of the Peruc-Korycany Formation (Bohemian Cretaceous Basin, Czech Republic). *International Geology Review* **53**, 1003–31. First published online: 29 December 2009.

CAVALCANTE, F., FIORE, S., LETTINO, A., PICCARRETA, G. & TATEO, F. 2007. Illite-Smectite mixed layer in Sicilide shales and piggy-back deposits of the Gorgoglione Formation (Southern Apennines): geological inferences. *Bollettino della Società Geologica Italiana* **103**, 241–54.

CAVALCANTE, F., FIORE, S., PICCARRETA, G. & TATEO, F. 2003. Geochemical and mineralogical approaches to assessing provenance and deposition of shales: a case study. *Clay Minerals* **38**, 383–97.

CONDIE, K. C. & WRONKIEWICZ, D. J. 1990. The Cr/Th ratio in Precambrian pelites from the Kaapvaal craton as an index of craton evolution. *Earth and Planetary Science Letters* **90**, 256–67.

COX, R. & LOWE, D. R. 1995. A conceptual review of regional-scale controls on the composition of clastic sediment and the co-evolution of continental blocks and their sediment cover. *Journal of Sedimentary Research* **1**, 1–12.

CRITELLI, S. 1999. The interplay of lithospheric flexure and thrust accomodation in forming stratigraphic sequences in the Southern Apennines foreland basin system, Italy. *Rendiconti di Scienze Fisiche e Naturali dell'Accademia Nazionale dei Lincei* **10**, 257–326.

CRITELLI, S., DE ROSA, R., SONNINO, M. & ZUFFA, G. G. 1990. Significato dei depositi vulcanoclastici della formazione delle Tufiti di Tusa (Miocene inferiore, Lucania meridionale). *Bollettino della Società Geologica Italiana* **109**, 743–62.

CRITELLI, S. & LE PERA, E. 1998. Post-Oligocene sediment-dispersal systems and unroofing history of the Calabrian microplate, Italy. *International Geology Review* **40**, 609–37.

CRITELLI, S., MONGELLI, G., PERRI, F., MARTÍN-ALGARRA, A., MARTÍN-MARTÍN, M., PERRONE, V., DOMINICI, R., SONNINO, M. & ZAGHLOUL, M. N. 2008. Compositional and geochemical signatures for the sedimentary evolution of the Middle Triassic–Lower Jurassic continental redbeds from Western–Central Mediterranean Alpine chains. *Journal of Geology* **116**, 375–86.

CULLERS, R. L. 2000. The geochemistry of shales, siltstones and sandstones of Pennsylvanian-Permian age, Colorado, USA: implications for provenance and metamorphic studies. *Lithos* **51**, 181–203.

DICKINSON, W. R. 1970. Interpreting detrital modes of greywacke and arkose. *Journal of Sedimentary Petrology* **40**, 695–707.

DICKINSON, W. R. 1985. Interpreting provenance relations from detrital modes of sandstones. In *Provenance of Arenites* (ed. G. G. Zuffa), pp. 333–61. Dordrecht: Reidel.

DOGLIONI, C., HARABAGLIA, P., MARTINELLI, G., MONGELLI, F. & ZITO, G. 1996. A geodynamic model of the Southern Apennines accretionary prism. *Terra Nova* **8**, 540–7.

FEDO, C. M., NESBITT, H. W. & YOUNG, G. M. 1995. Unraveling the effect of potassium metasomatism in sedimentary rocks and paleosols, with implications for paleoweathering conditions and provenance. *Geology* **23**, 921–4.

FENG, R. & KERRICH, R. 1990. Geochemistry of finegrained clastic sediments in the Archean Abitibi greenstones belt, Canada: implications for provenance and tectonic setting. *Geochimica et Cosmochima Acta* **54**, 1061–81.

FESNEAU, C., DECONINCK, J. F., PELLENARD, P. & REBOULET, S. 2009. Evidence of aerial volcanic activity during the Valanginian along the Northern Tethys margin. *Cretaceous Research* **30**, 533–9.

FLOYD, P. A. & LEVERIDGE, B. E. 1987. Tectonic environment of the Devonian Gramscatho basin, south Cornwall: framework mode and geochemical evidence from turbidite sandstones. *Journal of the Geological Society* **144**, 531–42.

FLOYD, P. A., WINCHESTER, J. A. & PARK, R. G. 1989. Geochemistry and tectonic setting of Lewisian clastic metasediments from the Early Proterozoic Loch Marse Group of Gairloch, N.W. Scotland. *Precambrian Research* **45**, 203–14

FRALICK, P. 2003. Geochemistry of clastic sedimentary rocks: ratio techniques. In *Geochemistry of Sediments and Sedimentary Rocks: Evolutionary Considerations*

to Mineral-Deposit-Forming Environments (ed. D. R. Lentz), pp. 85–104. Geological Association of Canada, GEOText, vol. 4.

FRANZINI, M., LEONI, L. & SAITTA, M. 1975. Revisione di una metodologia analitica per fluorescenza X basata sulla correzione degli effetti di matrice. *Rendiconti Società Italiana di Mineralogia e Petrologia* **31**, 365–78.

GARCIA, D., FONTEILLES, M. & MOUTTE, J. 1994. Sedimentary fractionations between Al, Ti, and Zr and the genesis of strongly peraluminous granites. *Journal of Geology* **102**, 411–22.

GUERRERA, F., MARTÍN-ALGARRA, A. & PERRONE, V. 1993. Late Oligocene-Miocene syn-, late-orogenic successions in Western and Central Mediterranean Chains from the Betic Cordillera to the Southern Apennines. *Terra Nova* **5**, 525–44.

GUERRERA, F. & VENERI, F. 1989. Evidenze di attività vulcanica nei sedimenti neogenici e pleistocenici dell'Appennino: stato delle conoscenze. *Bollettino della Società Geologica Italiana* **108**, 121–60.

INGERSOLL, R. V., BULLARD, T. F., FORD, R. L., GRIMM, J. P., PICKLE, J. D. & SARES, S. W. 1984. The effect of grain size on detrital modes: a test of the Gazzi-Dickinson point-counting method. *Journal of Sedimentary Petrology* **54**, 103–16.

JOHNSSON, M. J. 2000. Tectonic assembly of east-central Alaska: evidence from Cretaceous–Tertiary sandstones of the Kandik River terrane. *Geological Society of American Bulletin* **112**, 1023–42.

KRUMM, S. 1996. WINFIT 1.2: version of November 1996 (The Erlangen geological and mineralogical software collection) of "WINFIT 1.0: a public domain program for interact ive profile-analysis under WINDOWS". XIII Conference on Clay Mineralogy and Petrology, Praha, 1994. *Acta Univers itatis Carolinae Geologica* **38**, 253–61.

LAMASKIN, T. A., DORSEY, R. J. & VERVOORT, J. D. 2008. Tectonic controls on mudrock geochemistry, Mesozoic rocks of eastern Oregon and western Idaho, U.S.A.: implications for cordilleran tectonics. *Journal of Sedimentary Research* **78**, 765–83.

LAVIANO, R. 1987. *Analisi mineralogica quantitativa di argille mediante diffrattometria di raggi X.* In *Procedure di analisi di materiali argillosi.* 1–2/06/1987, pp. 215–34. Roma: ENEA S. Teresa, Lerici (Sp); Ed.ENEA.

LENTINI, F., CARBONE, S., DI STEFANO, A. & GUARNIERI, P. 2002. Stratigraphical and structural constraints in the Lucanian Apennines (Southern Italy): tools for reconstructing the geological evolution. *Journal of Geodynamics* **34**, 141–58.

LEONI, L. & SAITTA, M. 1976. X-ray fluorescence analysis of 29 trace elements in rock and mineral standards. *Rendiconti Società Italiana di Mineralogia e Petrologia* **32**, 497–510.

MCLENNAN, S. M., HEMMING, D. K. & HANSON, G. N. 1993. Geochemical approaches to sedimentation, provenance and tectonics. *Geological Society of America Special Paper* **284**, 21–40.

MCLENNAN, S. M., TAYLOR, S. R. & HEMMING, S. R. 2006. Composition, differentiation, and evolution of continental crust: constraints from sedimentary rocks and heat flow. In *Evolution and Differentiation of the Continental Crust* (eds M. Brown & T. Rushmer), pp. 92–134. Cambridge: Cambridge University Press.

MERRIMAN, R. J. & PEACOR, D. R. 1999. Very low–grade metapelites: mineralogy, microfabrics and measuring reaction progress. In *Low-Grade Metamorphism* (eds M. Frey & D. Robinson), pp. 10–60. Oxford: Blackwell Sciences Ltd.

MITCHELL, R. L. & SHELDON, N. D. 2009. Weathering and paleosol formation in the 1.1 Ga Keweenawan Rift. *Precambrian Research* **168**, 271–83.

MONGELLI, G., CRITELLI, S., PERRI, F., SONNINO, M. & PERRONE, V. 2006. Sedimentary recycling, provenance and paleoweathering from chemistry and mineralogy of Mesozoic continental redbed mudrocks, Peloritani Mountains, Southern Italy. *Geochemical Journal* **40**, 197–209.

MOORE, D. M. & REYNOLDS, R. C. 1997. *X-Ray Diffraction and the Identification and Analysis of Clay Minerals*, 2nd ed. New York: Oxford University Press, 378 pp.

NESBITT, H. W. & YOUNG, G. M. 1982. Early Proterozoic climates and plate motions inferred from major element chemistry of lutites. *Nature* **299**, 715–17.

OGNIBEN, L. 1969. Schema introduttivo alla geologia del confine calabro-lucano. *Memorie della Società Geologica Italiana* **8**, 435–763.

PATACCA, E. & SCANDONE, P. 2007. Geology of the Southern Apennines. In *Results of the CROP Project, Sub-project CROP-04 Southern Apennines (Italy)* (eds A. Mazzotti, E. Patacca & P. Scandone), pp. 75–119. *Bollettino della Società Geologica Italiana (Italian Journal of Geosciences)* Special Issue no. 7.

PERRI, F. 2008. Clay mineral assemblage of the Middle Triassic-Lower Jurassic mudrocks from Western-Central Mediterranean Alpine Chains. *Periodico di Mineralogia* **77**, 23–40.

PERRI, F., CIRRINCIONE, R., CRITELLI, S., MAZZOLENI, P. & PAPPALARDO, A. 2008. Clay mineral assemblages and sandstone compositions of the Mesozoic Longobucco Group (north-eastern Calabria): implications for burial history and diagenetic evolution. *International Geology Review* **50**, 1116–31.

PERRI, F., CRITELLI, S., MONGELLI, G. & CULLERS, R. L. 2010. Sedimentary evolution of the Mesozoic continental redbeds using geochemical and mineralogical tools: the case of Upper Triassic to Lowermost Jurassic Monte di Gioiosa mudstones (Sicily, southern Italy). *International Journal of Earth Sciences*, doi:10.1007/s00531-010-0602-6.

PERRI, F., MONGELLI, G., SONNINO, M., CRITELLI, S. & PERRONE, V. 2005. Chemistry and mineralogy of mesozoic continental redbed mudrocks from the Calabrian Arc, Southern Italy: implication for provenance, paleoweathering and burial history. *Atti Ticinensi di Scienze della Terra* **10**, 103–6.

PERRONE, V., MARTÌN-ALGARRA, A., CRITELLI, S., DECANDIA, F. A., D'ERRICO, M., ESTÈVEZ, A., IANNACE, A., LAZZAROTTO, A., MARTÌN-MARTÌN, M., MARTÌN-ROJAS, I., MAZZOLI, S., MESSINA, A., MONGELLI, G., VITALE, S. & ZAGHLOUL, M. N. 2006. "Verrucano" and "Pseudoverrucano" in the central-western Mediterranean Alpine chains: palaeogeographic evolution and geodynamic significance. In *Geology and Active Tectonics of the Western Mediterranean Region and North Africa* (eds A. Chalouan & G. Moratti), pp. 1–43. Geological Society of London, Special Publication no. 262.

PESCATORE, T., RENDA, P., SCHIATTARELLA, M. & TRAMUTOLI, M. 1999. Stratigraphic and structural relationships between Meso-Cenozoic Lagonegro basin and coeval carbonate platform in Southern Apennines, Italy. *Tectonophysics* **315**, 269–86.

REYNOLDS, R. C. Jr. 1985. *NEWMOD: a computer program for the calculation of the basal diffraction intensities of mixed-layered clay minerals*. Hanover, New Hampshire: R. C. Reynolds.

ROSER, B. P., COOMBS, D. S., KORSCH, R. J. & CAMPBELL, J. D. 2002. Whole-rock geochemical variations and evolution of the arc-derived Murihiku Terrane, New Zealand. *Geological Magazine* **139**, 665–85.

SGROSSO, I. 1994. Sulla posizione del bacino di Lagonegro (Appennino centro-meridionale). *Bollettino della Società Geologica Italiana* **113**, 179–94.

SLACK, J. F. & STEVENS, B. P. J. 1994. Clastic metasediments of the Early Proterozoic Broken Hill Group, New South Wales, Australia: geochemistry, provenance, and metallogenic significance. *Geochimica et Cosmochimica Acta* **58**, 257–73.

STEVENSON, R. K., WHITTAKER, S. & MOUNTJOY, E. W. 2000. Geochemical and Nd isotopic evidence for sedimentary-source changes in the Devonian miogeocline of the southern Canadian Cordillera. *Geological Society of American Bulletin* **112**, 531–9.

TAYLOR, S. R. & MCLENNAN, S. M. 1985. *The Continental Crust: Its Composition and Evolution*. Oxford: Blackwell.

WINCHESTER, J. A. & FLOYD, P. A. 1977. Geochemical discrimination of different magma series and their differentiation products using immobile elements. *Chemical Geology* **20**, 325–43.

ZAGHLOUL, M. N., CRITELLI, S., PERRI, F., MONGELLI, G., PERRONE, V., SONNINO, M., TUCKER, M., AIELLO, M. & VENTIMIGLIA, C. 2010. Depositional systems, composition and geochemistry of Triassic rifted-continental margin redbeds of Internal Rif Chain, Morocco. *Sedimentology* **57**, 312–50.

ZIMMERMANN, U. & SPALLETTI, L. A. 2009. Provenance of the Lower Paleozoic Balcarce Formation (Tandilia System, Buenos Aires Province, Argentina): implications for paleogeographic reconstructions of SW Gondwana. *Sedimentary Geology* **219**, 7–23.

ZUFFA, G. G. 1980. Hybrid arenites: their composition and classification. *Journal of Sedimentary Petrology* **50**, 21–9.